

# PREDICTION OF FLOW-INDUCED NOISE IN TRANSPORT VEHICLES: DEVELOPMENT AND VALIDATION OF A COUPLED STRUCTURAL-ACOUSTIC ANALYTICAL FRAMEWORK

Joana da Rocha<sup>1</sup>, Afzal Suleman<sup>1</sup>, and Fernando Lau<sup>2</sup>

<sup>1</sup>Dept. of Mechanical Engineering, University of Victoria, PO Box 3055, Stn. CSC, Victoria, BC, Canada, V8W 3P6  
jdarocha@uvic.ca, suleman@uvic.ca

<sup>2</sup>Centro de Ciências e Tecnologias Aeronáuticas, Dept. de Engenharia Mecânica, Instituto Superior Técnico, Av. Rovisco Pais, Lisboa, Portugal, 1049-001 lau@ist.utl.pt

## ABSTRACT

In this study, a complete analytical model framework able to accurately predict the flow-induced noise in the interior of a transport vehicle cabin is presented. The mathematical model framework presented represents a coupled structural-acoustic system, consisted by a plate subjected to a random excitation or to flow-induced noise, and an acoustic enclosure representing the transport vehicle cabin. The coupled analytical model is developed using the contribution of both structural and acoustic natural modes. It is shown that the analytical framework can be used for the prediction of flow-induced noise for different types of transport vehicles, by changing some of the parameters, as shown by the good agreement between the analytical results and several experimental studies. The results indicate that the analytical model is sensitive to the measurement location, with the change in position significantly affecting the predicted interior noise levels, as should be expected. Different sizes for the acoustic enclosure, as well as different types of panels were investigated. This study demonstrates the importance of including the acoustic receiving room (i.e., the vehicle cabin) contribution in the analytical formulation, in order to accurately predict the noise transmission and interior noise levels.

## RESUME

Dans cette étude, un modèle analytique complet, capable de prédire avec précision le bruit à l'intérieur d'une cabine d'un véhicule de transport induite par l'écoulement externe, est présenté. Le modèle mathématique représente un système structurel-acoustique accouplé, qui consiste en une plaque avec une excitation aléatoire ou à l'excitation du écoulement turbulent, et une chambre acoustique qui représente la cabine du véhicule de transport. Le modèle analytique accouplé a été développé en considérant la contribution combinée des modes naturels de ces deux systèmes, structurel et acoustique. Il est démontré que le modèle analytique peut être utilisé pour prédire le bruit induit par l'écoulement externe dans différents types de véhicules de transport, en variant certains paramètres, tel que vérifié par la bonne concordance entre les resultants analytiques et les résultats des multiples études expérimentales. Les résultats indiquent que le modèle analytique est sensible à la variation du point de mesure, et que le changement de la position de mesure affecte significativement les niveaux de bruit intérieur prédit, comme cela était prévu. Différentes dimensions de chambres acoustiques, ainsi que différents types de panneaux ont été étudiés. Cette étude démontre l'importance d'inclure la contribution de la salle acoustique de réception (i.e., l'habitacle du véhicule) dans la formulation analytique, afin de prédire avec précision la transmission du bruit et les niveaux de bruit à l'intérieur.

## INTRODUCTION

The interior noise and vibration in the cabin of an aircraft is mostly generated by the external flow excitation and engine noise. In opposition of what happens during takeoff, where the engine noise is the dominant cabin noise source, during cruise flight the airflow sources are the major contribution for the interior noise. Early measurements performed in jet

transport aircraft by [1], have shown how the relative importance of engine and flow noise changes drastically during the course of a flight. This study concluded that, during takeoff and initial climb, the engine was the main source of cabin noise. However, during the climb to cruise flight altitude, the turbulent boundary layer (TBL) noise gradually increases and the engine noise decreases. Finally, when the cruise flight is reached, the TBL becomes the

dominant source of interior noise, resulting from the increase of flight speed, and there is a reduction of engine noise, as the engine thrust is reduced to cruise setting. Furthermore, as referred in [2], turbulent boundary layer excitation is regarded as the most important noise source for jet powered aircraft at cruise speed, particularly, as new quieter jet engines are being developed. Similarly, automotive industry is progressively more concerned with passengers comfort. Since major advances have been made to the reduction of sound transmitted to the interior from the engine, transmission, and tires, the reduction of flow-induced noise is becoming more important. Additionally, as concluded by several studies for subsonic flight, e.g. [3-5], turbulent boundary layer pressure levels on the exterior of the fuselage increases with the flight Mach number.

Nowadays, reduced cabin interior noise is an important factor when considering the design of aircraft and transport vehicles in general, and it will even become a more important issue in the future transport vehicles. Reduced levels of interior cabin noise are desirable for both comfort and health-related reasons, and they are balanced with the cost, complexity, and physical constraints of noise control systems. Passive noise control (PNC) techniques are not effective in the low-frequency noise (LFN) range, where the active noise control techniques (ANC and ASAC) have demonstrated better results, showing the ability to decrease sound levels without a big penalty in terms of weight, compared with the PNC solutions [6-9]. However, the successful implementation of noise control techniques is a challenging problem, and is far from being a straightforward task. The complexity of the physics of the structural-acoustic coupled system itself, consisting of the fuselage structure together with the cabin interior, is already a major difficulty for solving the problem. To efficiently design a noise control system, a clear understanding of the mechanisms of sound radiation and transmission of the coupled structural-acoustic system is crucial. Furthermore, when considering the TBL excitation, the noise reduction problem turns into even more complicated, since the turbulent boundary layer induced pressure has a random and broadband nature.

Early experimental tests have been conducted as an effort to characterize the radiation of sound from single panels excited by turbulent boundary layers [4, 10-15]. The results illustrate that the TBL is a major source of exterior pressure fluctuations and provide knowledge about the shape of the spectrum, convection velocity and space-time correlation of the turbulent boundary layer pressure fluctuations on aircraft panels, as well as displacement and acceleration spectra of the vibrating aircraft panels. In addition, theoretical studies have been performed for the vibration and sound radiated by isolated panels (i.e., not coupled with an acoustic enclosure) excited by turbulent flows [16-20], and for random vibration of a plate coupled with acoustic enclosures [2, 21, 22]. In these studies, when the TBL excitation is object of study, it is usually described in terms of the statistical properties of the wall pressure fluctuations based on the Corcos

formulation [23, 24]. A number of new models were developed after Corcos model for the TBL statistical description [25-29]. The main limitation of the Corcos formulation is the assumption that spanwise and streamwise correlations lengths do not depend on the boundary layer thickness parameter, unlike other methods. Despite not being the most accurate, the Corcos model is widely used to describe the induced TBL pressure field, since it captures the fundamental pressure tendency along the frequency and requires significantly reduced computational effort to employ. In the other hand, the Corcos-like formulation provides a good estimation for the TBL wall-pressure fluctuations levels at and near the convective peak, which is of fundamental importance for aircraft boundary layers (for high subsonic Mach numbers) [30]. Finally, with the Corcos model it is possible to obtain analytical expressions for the response of simply supported panel, which is fundamental in the present study. For all these reasons, the Corcos formulation is still being used in recent studies to describe the TBL wall-pressure fluctuations, e.g., [2, 30-36].

As a physical problem, the TBL-induced noise into a cabin can be simply explained as follows: (1) the turbulent boundary layer pressure fluctuations induce vibrations on the cabin structure, and (2) the vibrating structure radiates noise into the cabin. Mathematically, this physical problem can be simulated by the interaction of three different models: (1) an aerodynamic model, representing the TBL pressure fluctuations on the cabin structure; (2) a structural model, which characterize the vibration of the cabin structure; and (3) an acoustic model that represents the cabin interior sound pressure level.

The main goal of the current investigation is the development of an accurate analytical framework for the prediction TBL-induced noise into transport vehicles cabins, and its validation. The knowledge of the characteristics of the turbulent boundary layer excitation, its induced vibration on the structure, and the noise radiated into the cabin space is essential for the accurate prediction of the interior noise levels. The effect of the receiving room space, i.e. the cabin space, is an important factor for the accurate interior noise prediction, as shown by the results shown in this study.

For the validation of the analytical framework, four studies were considered for comparison, more specifically the investigations by [2, 8, 22, 37]. The acoustic enclosure is of rectangular shape, filled with air, with five rigid walls and one wall completely or partially flexible. The flexible part of the enclosure wall is backed by the turbulent boundary layer or by normally impinging random noise. The analytical expressions obtained in this study, shown in the Appendices section, are able to predict overall values of interior SPL, overall values of plate vibration levels, as well as the SPL at a chosen point in the interior of the enclosure, and the level of structural vibration at a given point of the structure. The spectral quantities were obtained for frequencies up to 1000 Hz. The analytical framework here

validated can be used to predict cabin noise for more complex cases, as the case shown [38].

The present article is organized as follows. First, the concepts and models used in the study are formally described. Section 2 presents the turbulent boundary layer wall pressure fluctuations model, Section 3 the structural model, Section 4 the acoustic model, and Section 5 the coupled structural-acoustic model. The method of solution for the prediction of the spectral quantities is discussed in Section 6. Section 7 provides a discussion of the results obtained using the developed analytical framework, and their validation with the results from the literature. Finally, a summary of the results and concluding remarks are presented.

## 2. TURBULENT BOUNDARY LAYER WALL PRESSURE FIELD MODEL

The prediction of the vibration and sound of a flow-excited structure is dependent on a good description of the wall pressure field. Since numerical predictions are limited to low Reynolds number simple flow, one has to rely on semi-empirical models fitted to experimental data. Modeling the turbulent boundary layer wall pressure has been a subject of study for many years. As previously referred in this report, a large number of empirical models have been developed to describe the wall pressure fluctuations on a flat plate wall due to the TBL. The turbulent boundary layer wall pressure,  $p(x, y, t)$ , is usually statistically described in terms of the pressure power spectral density,  $S(s_1, s_2, \omega)$ , where  $s_1$  is the current position along the plate, and  $s_2$  the separation vector between two measurement points.

In general, for a fully developed TBL, and for zero mean pressure gradient, the turbulent flow can be regarded as stationary and homogeneous in space, so that the  $s_1$  dependence disappears in the  $S(s_1, s_2, \omega)$  function. This way, for turbulent flow in the  $x$ -direction, the cross power spectral density (PSD) of the wall pressure over the  $(x, y)$  plane, can be defined as

$$S(\xi_x, \xi_y, \omega) = \langle p^*(x, y, \omega), p(x - \xi_x, y - \xi_y, \omega) \rangle, \quad (1)$$

in which  $\xi_x = x - x'$  and  $\xi_y = y - y'$  are the spatial separations in the streamwise and spanwise directions of the plate, respectively. Also, the cross PSD of a stationary random process can be expressed as the product of a reference PSD function,  $S_{\text{ref}}(\omega)$ , and a spatial correlation function,  $\bar{S}(\xi_x, \xi_y, \omega)$ , as

$$S(\xi_x, \xi_y, \omega) = S_{\text{ref}}(\omega) \bar{S}(\xi_x, \xi_y, \omega). \quad (2)$$

Corcos [23, 24], proposed a model which considers the cross power spectral density of the stationary and homogeneous TBL wall pressure field in a separate form in the streamwise,  $x$ -, and spanwise,  $y$ -direction, as

$$S(\xi_x, \xi_y, \omega) = S_{\text{ref}}(\omega) f_1\left(\frac{\omega \xi_x}{U_c}\right) f_2\left(\frac{\omega \xi_y}{U_c}\right) e^{-i\omega \xi_x / U_c}, \quad (3)$$

where  $U_c$  is the TBL convective speed. Corcos found that measurements of particular forms of the cross PSD  $S(\xi_x, 0, \omega)$  and  $S(0, \xi_y, \omega)$  could be well represented as functions of the variables  $(\omega \xi_x / U_c)$  and  $(\omega \xi_y / U_c)$ , respectively. In practice, the functions  $f_1(\omega \xi_x / U_c)$  and  $f_2(\omega \xi_y / U_c)$  are frequently approximated by exponential decay functions, i.e.

$$S(\xi_x, \xi_y, \omega) = S_{\text{ref}}(\omega) e^{-\frac{\alpha_x \omega |\xi_x|}{U_c}} e^{-\frac{\alpha_y \omega |\xi_y|}{U_c}} e^{-i\omega \xi_x / U_c}, \quad (4)$$

where  $\alpha_x$  and  $\alpha_y$  are empirical parameters, chosen to yield the best agreement with the reality, which denote the loss of coherence in the longitudinal and transverse directions. Usually,  $\alpha_x \in [0.1; 0.12]$  and  $\alpha_y \in [0.7; 1.2]$ . Recommended empirical values for aircraft boundary layers are  $\alpha_x = 0.1$  and  $\alpha_y = 0.77$  [39]. For the reference power spectrum,  $S_{\text{ref}}(\omega)$ , all the chosen studies for the validation of our model provide information about its value. However, in case of the absence of an adequate reference power spectrum function or value, the authors anticipate that the model proposed by Efimtsov [25] provides a good agreement with experimental data for the case of an aircraft in cruise flight [39, 40].

## 3. STRUCTURAL MODEL

Generally, an aircraft fuselage is a conventional skin-stringer-frame structure, with several panels connected between adjacent stringers and frames. Each individual panel can be assumed to vibrate independently of each other. As concluded in [13, 14], while jet noise induced vibration in aircraft is highly correlated over several aircraft panels, in both longitudinal and circumferential directions, the TBL induced vibration (in which the vibration correlation decays rapidly especially in the circumferential direction) is confined to one or two adjacent panels in the longitudinal direction.

The panels are considered to be flat and simply supported in all four boundaries. With these conditions, the vibration of an individual panel can be defined as [41, 42]

$$w(x, y, t) = \sum_{m_x=1}^{M_x} \sum_{m_y=1}^{M_y} \alpha_{m_x}(x) \beta_{m_y}(y) q_{m_x m_y}(t), \quad (5)$$

in which  $\alpha_{m_x}(x)$  and  $\beta_{m_y}(y)$  are the spatial functions, defining the variation of  $w(x, y, t)$  with the variables  $x$  and  $y$  respectively,  $q_{m_x m_y}(t)$  functions define the variation of  $w(x, y, t)$  with time, and  $M = M_x \times M_y$  is the total number of plate modes  $(m_x, m_y)$  considered for the analysis. For simply supported plates, the spatial functions can be defined as:

$$\alpha_{m_x}(x) = \sqrt{\frac{2}{a}} \sin\left(\frac{m_x \pi x}{a}\right), \quad (6a)$$

$$\beta_{m_y}(y) = \sqrt{\frac{2}{b}} \sin\left(\frac{m_y \pi y}{b}\right), \quad (6b)$$

where  $a$  and  $b$  are the length and width of the plate, respectively. The natural frequencies of the simply supported panel are given by

$$\omega_{m_x m_y}^p = \sqrt{\frac{D_p}{\rho_p h_p} \left[ \left(\frac{m_x \pi}{a}\right)^2 + \left(\frac{m_y \pi}{b}\right)^2 \right]}, \quad (7)$$

in which  $\rho_p$  is the density of the panel,  $h_p$  is its thickness, and  $D_p = \frac{E_p h_p^3}{12(1-\nu_p^2)}$  is the panel stiffness constant, with  $E_p$  being the panel Elasticity modulus and  $\nu_p$  the Poisson ratio. The plate governing equation, for a given applied external pressure, is defined as

$$D_p \nabla^4 w + \rho_p h_p \ddot{w} + \zeta_p \dot{w} = p_{\text{ext}}(x,y,t), \quad (8)$$

in which the term  $\zeta_p$  was added to account for the damping of the plate.

#### 4. ACOUSTIC MODEL

The acoustical physical system consists of a three-dimensional rectangular enclosure, with five fixed walls, and one totally or partially flexible wall. Similarly to the description of plate vibration in the structural model, the pressure field inside the acoustic enclosure can be defined through the acoustic modes, as following [43, 44]

$$p(x,y,z,t) = \sum_{n_x=1}^{N_x} \sum_{n_y=1}^{N_y} \sum_{n_z=1}^{N_z} \psi_{n_x}(x) \phi_{n_y}(y) \Gamma_{n_z}(z) r_{n_x n_y n_z}(t), \quad (9)$$

in which  $\psi_{n_x}(x)$ ,  $\phi_{n_y}(y)$  and  $\Gamma_{n_z}(z)$  are the spatial functions, defining the variation of  $p(x,y,z,t)$  with the variables  $x$ ,  $y$  and  $z$  respectively,  $r_{n_x n_y n_z}(t)$  functions define the variation of  $p(x,y,z,t)$  with time, and  $N = N_x \times N_y \times N_z$  is the total number of plate modes ( $n_x$ ,  $n_y$ ,  $n_z$ ) considered. The spatial functions are assumed to be orthogonal between each other, and are given by the rigid body enclosure modes [45, 46], i.e.:

$$\psi_{n_x}(x) = \frac{A_{n_x}}{\sqrt{L_x}} \cos\left(\frac{n_x \pi x}{L_x}\right), \quad (10a)$$

$$\phi_{n_y}(y) = \frac{A_{n_y}}{\sqrt{L_y}} \cos\left(\frac{n_y \pi y}{L_y}\right), \quad (10b)$$

$$\Gamma_{n_z}(z) = \frac{A_{n_z}}{\sqrt{L_z}} \cos\left(\frac{n_z \pi z}{L_z}\right). \quad (10c)$$

where  $L_x$ ,  $L_y$  and  $L_z$  are the dimensions of the acoustic enclosure in the  $x$ -,  $y$ - and  $z$ - direction, respectively, and constants  $A_n$  were chosen in order to satisfy normalization. It can be shown that:

$$A_n = \begin{cases} \sqrt{2}, & \text{for } n \neq 0 \\ 1, & \text{for } n = 0. \end{cases} \quad (11)$$

The natural frequencies of a rectangular cavity can be determined using the following equation [45]

$$\omega_{n_x n_y n_z}^{\text{ac}} = c_0 \sqrt{\left(\frac{n_x \pi}{L_x}\right)^2 + \left(\frac{n_y \pi}{L_y}\right)^2 + \left(\frac{n_z \pi}{L_z}\right)^2}, \quad (12)$$

in which  $c_0$  is the speed of sound inside the acoustic enclosure. The governing equation of this subsystem is the wave equation, defined by

$$\nabla^2 p - \frac{1}{c_0^2} \ddot{p} - \zeta_{\text{ac}} \dot{p} = 0, \quad (13)$$

where the damping term  $\zeta_{\text{ac}}$  was added to account for the acoustic damping in the enclosure.

#### 5. STRUCTURAL-ACOUSTIC MODEL

The governing equations for the coupled structural acoustic system are obtained from the combination of the previously described governing equations for the individual uncoupled systems. To perform that combination, some mathematical manipulation is needed.

First, considering the plate governing equation, the right-hand side of Eq.(8) may be divided in two different contributions: (1) the external TBL excitation,  $p_{\text{tbl}}(x, y, t)$ , applied in the upper part of the panel, and (2) the pressure field,  $p(x,y,z=L_z,t)$ , applied in the panel due to the acoustic enclosure contribution. Considering this, Eq.(8) can be re-written as

$$D_p \nabla^4 w + \rho_p h_p \ddot{w} + \zeta_p \dot{w} = p(x,y,z=L_z,t) - p_{\text{tbl}}(x,y,t). \quad (14)$$

Substituting  $w(x,y,t)$  in Eq.(14) by the expression defined in Eq.(5), expressing  $p(x,y,z=L_z,t)$  in terms of Eqs.(9) and (10), making use of the orthogonality of the plate modes, and integrating the entire equation over the plate area, Eq.(14) becomes

$$\begin{aligned} \rho_p h_p \left\{ \ddot{q}_m(t) + 2 \omega_m \zeta_p \dot{q}_m(t) + \omega_m^2 q_m(t) \right\} = \\ \sum_{n=1}^N \frac{(-1)^{n_z} A_{n_z}}{\sqrt{L_z}} \int_{x_{p1}}^{x_{pF}} \alpha_{m_x}(x) \psi_{n_x}(x) dx \int_{y_{p1}}^{y_{pF}} \beta_{m_y}(y) \phi_{n_y}(y) dy r_n(t) \\ - \int_{y_{p1}}^{y_{pF}} \int_{x_{p1}}^{x_{pF}} \alpha_{m_x}(x) \beta_{m_y}(y) p_{\text{tbl}}(x,y,z=L_z,t) dx dy, \end{aligned} \quad (15)$$

where  $\zeta_p = 2 \omega_m \zeta_p$  is the structural modal damping;  $x_{p_i}$  and  $x_{p_f}$  are, respectively, the initial and last x-coordinates of the plate (corresponding to the plate length);  $y_{p_i}$  and  $y_{p_f}$  are, respectively, the initial and last y-coordinates of the plate (plate width); and  $\omega_{m_x m_y}^p$ ,  $q_{m_x m_y}(t)$ , and  $r_{n_x n_y n_z}(t)$  were substituted, respectively, by  $\omega_m$ ,  $q_m(t)$  and  $r_n(t)$ , for notation simplicity.

Second, considering the rectangular acoustic enclosure governing equation, Eq.(13), the boundary conditions may be defined as follows: (1) normal component of the air particle velocity equal to zero at the enclosure rigid walls, and (2) equal to normal velocity of the panel, at the flexible wall, i.e.,

$$\frac{\partial p}{\partial u} = \begin{cases} -\rho_0 \ddot{w}, & \text{at } z = L_z \\ 0, & \text{at rigid boundaries,} \end{cases} \quad (16)$$

in which  $u$  represents the direction normal to the boundary, and  $\rho_0$  is the air density into the acoustic enclosure.

Substituting Eqs.(10) and (11) into Eq.(9), and then into Eq.(13), making use of the orthogonality condition of the acoustic modes, integrating over the volume of the rectangular enclosure, and, finally, applying the boundary conditions given by Eq.(16), the rectangular enclosure governing equation Eq.(13) becomes

$$\frac{1}{c_0^2} \{ \ddot{r}_n(t) + 2 \omega_n \zeta_{ac} \dot{r}_n(t) + \omega_n^2 r_n(t) \} = -\rho_0 \frac{(-1)^{n_z} A_{n_z}}{\sqrt{L_z}} \sum_{m=1}^M \int_{x_{p_i}}^{x_{p_f}} \alpha_{m_x}(x) \psi_{n_x}(x) dx \int_{y_{p_i}}^{y_{p_f}} \beta_{m_y}(y) \phi_{n_y}(y) dy \ddot{q}_m(t) \quad (17)$$

where  $\zeta_{ac} = 2 \omega_n \zeta_{ac}$  is the acoustic modal damping, and  $\omega_{n_x n_y n_z}^{ac}$ ,  $r_{n_x n_y n_z}(t)$ , and  $q_{m_x m_y}(t)$  were substituted, respectively, by  $\omega_n$ ,  $r_n(t)$  and  $q_m(t)$ , for notation simplicity. Note that the term on the right-hand side of Eq.(17) and the first term on the right-hand side of Eq.(15) represent the coupling between the structural vibration and the enclosure acoustic pressure.

Third, it is convenient to write the couple system governing equations, Eqs.(15) and (17), together into the following matrix form:

$$\begin{bmatrix} \mathbf{M}_{pp} & \mathbf{0} \\ \mathbf{M}_{cp} & \mathbf{M}_{cc} \end{bmatrix} \begin{Bmatrix} \ddot{\mathbf{q}}(t) \\ \ddot{\mathbf{r}}(t) \end{Bmatrix} + \begin{bmatrix} \mathbf{D}_{pp} & \mathbf{0} \\ \mathbf{0} & \mathbf{D}_{cc} \end{bmatrix} \begin{Bmatrix} \dot{\mathbf{q}}(t) \\ \dot{\mathbf{r}}(t) \end{Bmatrix} + \begin{bmatrix} \mathbf{K}_{pp} & \mathbf{K}_{pc} \\ \mathbf{0} & \mathbf{K}_{cc} \end{bmatrix} \begin{Bmatrix} \mathbf{q}(t) \\ \mathbf{r}(t) \end{Bmatrix} = \begin{Bmatrix} \mathbf{P}_{tbl}(t) \\ \mathbf{0} \end{Bmatrix}, \quad (18)$$

in which:

$$\mathbf{M}_{pp} = \text{diag} [\rho_p h_p] \quad \text{and} \quad \mathbf{M}_{cc} = \text{diag} \left[ \frac{1}{c_0^2} \right], \quad (19a)$$

$$\mathbf{M}_{cp} = \rho_0 \left[ \frac{(-1)^{n_z} A_{n_z}}{\sqrt{L_z}} \int_{x_{p_i}}^{x_{p_f}} \alpha_{m_x}(x) \psi_{n_x}(x) dx \int_{y_{p_i}}^{y_{p_f}} \beta_{m_y}(y) \phi_{n_y}(y) dy \right], \quad (19b)$$

$$\mathbf{D}_{pp} = \text{diag} [2\rho_p h_p \omega_m \zeta_p] \quad \text{and} \quad \mathbf{D}_{cc} = \text{diag} \left[ 2 \frac{1}{c_0^2} \omega_n \zeta_{ac} \right], \quad (19c)$$

$$\mathbf{K}_{pp} = \text{diag} [\omega_m^2 \rho_p h_p] \quad \text{and} \quad \mathbf{K}_{cc} = \text{diag} \left[ \omega_n^2 \frac{1}{c_0^2} \right], \quad (19d)$$

$$\mathbf{K}_{pc} = - \left[ \frac{(-1)^{n_z} A_{n_z}}{\sqrt{L_z}} \int_{x_{p_i}}^{x_{p_f}} \alpha_{m_x}(x) \psi_{n_x}(x) dx \int_{y_{p_i}}^{y_{p_f}} \beta_{m_y}(y) \phi_{n_y}(y) dy \right], \quad (19e)$$

$$\mathbf{p}_{tbl}(t) = - \left[ \int_{y_{p_i}}^{y_{p_f}} \int_{x_{p_i}}^{x_{p_f}} \alpha_{m_x}(x) \beta_{m_y}(y) p_{tbl}(x,y,z=L_z,t) dx dy \right]. \quad (19f)$$

In these equations,  $\mathbf{M}$  corresponds to mass matrices,  $\mathbf{D}$  to damping matrices,  $\mathbf{K}$  to stiffness matrices, and subscripts  $p$  and  $c$  represent respectively *plate* and *cavity*, with:  $\mathbf{M}_{pp}$ ,  $\mathbf{D}_{pp}$ , and  $\mathbf{K}_{pp} \in \mathfrak{R}^{M \times M}$ ;  $\mathbf{M}_{cc}$ ,  $\mathbf{D}_{cc}$  and  $\mathbf{K}_{cc} \in \mathfrak{R}^{N \times N}$ ;  $\mathbf{M}_{cp} \in \mathfrak{R}^{N \times M}$ ;  $\mathbf{K}_{pc} \in \mathfrak{R}^{M \times N}$ ;  $\mathbf{q}(t)$  and  $\mathbf{p}_{tbl}(t) \in \mathfrak{R}^{M \times 1}$ ; and  $\mathbf{r}(t) \in \mathfrak{R}^{N \times 1}$ . All matrices and vectors expressions were obtained analytically. Appendix A contains final analytical expressions derived for  $\mathbf{M}_{cp}$  and  $\mathbf{K}_{pc}$  matrices.

Since the TBL wall pressure field model, described in section 2 of this article, is expressed in the frequency domain, it is opportune to transform Eq.(18) from the time domain to the frequency domain. For this purpose, one may assume the components of the time functions defined as  $q_m = Q_m e^{i\omega t}$  and  $r_n = R_n e^{i\omega t}$ . Using this form of the time function, Eq.(18) can be written in frequency domain as

$$\mathbf{Y}(\omega) = \mathbf{H}(\omega) \mathbf{X}(\omega), \quad (19)$$

in which the  $\mathbf{Y}(\omega)$  is the response of the system to the excitation  $\mathbf{X}(\omega)$ , and  $\mathbf{H}(\omega)$  is the frequency response matrix of the system, and are defined, respectively, by:

$$\mathbf{Y}(\omega) = \begin{Bmatrix} \mathbf{W}(\omega) \\ \mathbf{P}(\omega) \end{Bmatrix} \quad \text{and} \quad \mathbf{X}(\omega) = \begin{Bmatrix} \mathbf{P}_{tbl}(\omega) \\ \mathbf{0} \end{Bmatrix}, \quad (20a)$$

$$\mathbf{H}(\omega) = \begin{bmatrix} -\omega^2 \mathbf{M}_{pp} + i\omega \mathbf{D}_{pp} + \mathbf{K}_{pp} & \mathbf{K}_{pc} \\ -\omega^2 \mathbf{M}_{cp} & -\omega^2 \mathbf{M}_{cc} + i\omega \mathbf{D}_{cc} + \mathbf{K}_{cc} \end{bmatrix}^{-1}. \quad (20b)$$

In these equations, vectors  $\mathbf{W}(\omega)$ ,  $\mathbf{P}(\omega)$  and  $\mathbf{P}_{tbl}(\omega)$  correspond to the frequency domain vectors of the previously defined time domain vectors  $\mathbf{w}(t)$ ,  $\mathbf{p}(t)$  and  $\mathbf{p}_{tbl}(t)$ , respectively.

## 6. METHOD FOR SOLUTION

One last step, needed to obtain a solution for the problem, is to transform the coupled system equations to PSD domain, as the TBL wall pressure model available is written in terms of the power spectral density of the wall pressure. This way, considering the TBL random excitation as a stationary and homogeneous function, the spectral density of the system response,  $S_{YY}(\omega)$ , is defined by [47, 48]

$$S_{YY}(\omega) = \mathbf{H}^*(\omega) S_{XX}(\omega) \mathbf{H}^T(\omega), \quad (21)$$

where  $S_{XX}(\omega)$  is the PSD matrix of the random excitation,  $\mathbf{X}(\omega)$ ,  $S_{YY}(\omega)$  is the PSD matrix of the random response,  $\mathbf{Y}(\omega)$ , and superscripts \* and T denote Hermitian conjugate and matrix transpose, respectively. It is convenient to write the system response matrix,  $\mathbf{H}(\omega)$ , defined by Eq.(20b), in the following form

$$\mathbf{H}(\omega) = \begin{bmatrix} \mathbf{A} & \mathbf{B} \\ \mathbf{C} & \mathbf{D} \end{bmatrix}^{-1}, \quad (22)$$

with:

$$\mathbf{A} = -\omega^2 \mathbf{M}_{pp} + i \omega \mathbf{D}_{pp} + \mathbf{K}_{pp}, \quad (23a)$$

$$\mathbf{B} = \mathbf{K}_{pc}, \quad (23b)$$

$$\mathbf{C} = -\omega^2 \mathbf{M}_{cp}, \quad (23c)$$

$$\mathbf{D} = -\omega^2 \mathbf{M}_{cc} + i \omega \mathbf{D}_{cc} + \mathbf{K}_{cc}. \quad (23d)$$

Also, for mathematical calculations, it is opportune to divide the matrix  $S_{YY}(\omega)$  into two matrices: (1) the PSD matrix of the coupled plate displacement,  $S_{WW}(\omega)$ , and (2) the PSD matrix of the coupled acoustic pressure,  $S_{PP}(\omega)$ . Similarly, the matrix  $S_{XX}(\omega)$  may be divided in two: (1) the PSD matrix of the TBL pressure, and (2) a null matrix. With this manipulation, Eq.(21) can be written in a separate form, defining matrices  $S_{WW}(\omega)$  and  $S_{PP}(\omega)$ , independently, as functions of the PSD matrix of the TBL excitation,  $S_{tbl}(\omega)$ , respectively, as follows:

$$S_{WW}(\omega) = \mathbf{H}_W^*(\omega) S_{tbl}(\omega) \mathbf{H}_W^T(\omega), \quad (24)$$

and

$$S_{PP}(\omega) = \mathbf{H}_P^*(\omega) S_{tbl}(\omega) \mathbf{H}_P^T(\omega), \quad (25)$$

in which matrices the  $\mathbf{H}_W(\omega)$  and  $\mathbf{H}_P(\omega)$  are defined, respectively, by:

$$\mathbf{H}_W(\omega) = (\mathbf{A} - \mathbf{B} \mathbf{D}^{-1} \mathbf{C})^{-1}, \quad (26)$$

and

$$\mathbf{H}_P(\omega) = -\mathbf{D}^{-1} \mathbf{C} \mathbf{H}_W(\omega). \quad (27)$$

The generalized PSD matrix of the TBL excitation,  $S_{tbl}(\omega) \in \mathfrak{R}^{M \times M}$ , is defined as follows

$$S_{tbl}(\omega) = \left[ \int_{y_{p1}}^{y_{pf}} \int_{x_{p1}}^{x_{pf}} \int_{y_{p1}}^{y_{pf}} \int_{x_{p1}}^{x_{pf}} \alpha_{m_x}(x) \alpha_{m_x}(x') \beta_{m_y}(y) \beta_{m_y}(y') S(\xi_x, \xi_y, \omega) dx dx' dy dy' \right], \quad (28)$$

in which  $S(\xi_x, \xi_y, \omega)$  is defined by Eq.(4). The analytically expression obtained for the matrix  $S_{tbl}(\omega)$  can be seen in Appendix B. Finally, the PSD functions of the plate displacement and acoustic enclosure pressure can be defined using the previously defined PSD matrices, respectively as:

$$S_{ww}(x_1, y_1, x_2, y_2, \omega) = \sum_{m_{x1}, m_{x2}=1}^{M_x^2} \sum_{m_{y1}, m_{y2}=1}^{M_y^2} \alpha_{m_{x1}}(x_1) \alpha_{m_{x2}}(x_2) \beta_{m_{y1}}(y_1) \beta_{m_{y2}}(y_2) S_{ww}(\omega)_{m_1, m_2} \quad (29)$$

and

$$S_{pp}(x_1, y_1, z_1, x_2, y_2, z_2, \omega) = \sum_{n_{x1}, n_{x2}=1}^{N_x^2} \sum_{n_{y1}, n_{y2}=1}^{N_y^2} \sum_{n_{z1}, n_{z2}=1}^{N_z^2} \psi_{n_{x1}}(x_1) \psi_{n_{x2}}(x_2) \phi_{n_{y1}}(y_1) \phi_{n_{y2}}(y_2) \Gamma_{n_{z1}}(z_1) \Gamma_{n_{z2}}(z_2) S_{pp}(\omega)_{n_1, n_2} \quad (30)$$

Eqs.(29) and (30) can be used, respectively, to calculate the displacement PSD at a certain point in the plate, and the pressure PSD at any given location of the acoustic enclosure. If one desires to predict the auto-spectral density solutions, for instance, at the location 1, it can be calculated by replacing  $x_2$  by  $x_1$ ,  $y_2$  by  $y_1$ , and  $z_2$  by  $z_1$  in Eqs.(29) and (30). The overall PSD functions are calculated by integrating the individual PSD functions over the plate area and the cavity volume, respectively, as following:

$$S_{ww}(\omega) = \int_{y_{p1}}^{y_{pf}} \int_{x_{p1}}^{x_{pf}} \int_{y_{p1}}^{y_{pf}} \int_{x_{p1}}^{x_{pf}} S_{ww}(x_1, y_1, x_2, y_2, \omega) dx_1 dx_2 dy_1 dy_2, \quad (31)$$

and

$$S_{pp}(\omega) = \int_{z_{c1}}^{z_{cf}} \int_{y_{c1}}^{y_{cf}} \int_{x_{c1}}^{x_{cf}} S_{pp}(x_1, y_1, z_1, x_2, y_2, z_2, \omega) dx_1 dx_2 dy_1 dy_2 dz_1 dz_2. \quad (32)$$

in which  $x_{c1}$  and  $x_{cf}$  are, respectively, the initial and last x-coordinates of the acoustic enclosure (corresponding to the enclosure length);  $y_{c1}$  and  $y_{cf}$  are, respectively, the initial and last y-coordinates of the enclosure (enclosure width); and  $z_{c1}$  and  $z_{cf}$  are, respectively, the initial and last z-coordinates of the enclosure (enclosure height). The final analytical

expressions derived for  $S_{ww}(\omega)$  and  $S_{pp}(\omega)$  are shown in Appendix C.

## 7. VALIDATION OF THE MODEL

### 7.1 Validation Case 1

The study documented in [22] performed by NASA, presents an experimental and theoretical study with different panels in order to determine the noise transmission in a coupled panel-cavity system. The analytical model presented is a simple, one-dimensional model, providing a good fitting with the experimental results trend line. The noise sources considered were normally impinging sine waves (with an amplitude of 110 dB) and normally incident random noise (a white noise source providing 120 dB sound pressure level).

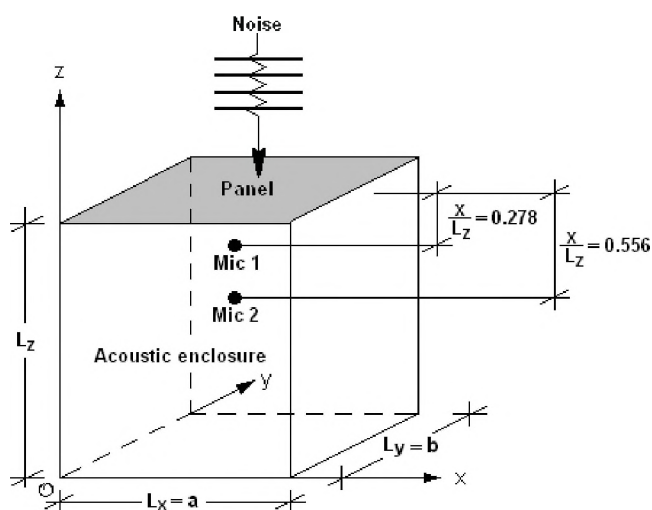


Figure 1. Details of the physical system of validation case 1.

Table 1. Parameters of the physical system for validation case 1.

Plate Properties (PVC)		
Variable	Description	Value
$\rho_p$	Density	1562.5 Kg m <sup>-3</sup>
$E_p$	Elasticity Modulus	3.2×10 <sup>9</sup> Pa <sup>2</sup>
$\nu$	Poisson's ratio	0.41
$\xi_{sp}$	Damping ratio	0.02
$h_p$	Thickness	0.0016 m
$a$	Length	0.305 m
$b$	Width	0.381 m
Acoustic Enclosure Properties (Air)		
Variable	Description	Value
$c_0$	Speed of sound	348 m s <sup>-1</sup>
$\xi_{ac}$	Damping ratio	0.001
$L_x$	Length	0.305 m
$L_y$	Width	0.381 m
$L_z$	Height	0.454 m

This study was considered as the validation case 1, and the system is composed by a PVC (Lead impregnated polyvinylchloride) panel coupled with a hard walled

acoustic cavity, as shown in Fig. 1. The main properties of the system are displayed in Table 1. Two measurement microphones were located inside the cavity, directly behind the flexible panel, as shown in Fig. 1, in order to provide measurements of the interior sound pressure level. The noise reduction, NR, was obtained as following

$$NR = -10 \log_{10} \left( \frac{S_{pp}}{S_{ext}} \right), \quad (33)$$

in which,  $S_{pp}$  is the pressure PSD at the location of the interior microphone and  $S_{ext}$  is the external pressure PSD. Using our analytical framework,  $S_{pp}$  can be calculated from Eq.(30), while  $S_{ext}$  corresponds to  $S_{ref}$  expressed in Eqs. (2) to (4).

Figs. 2 and 3 show the noise reduction results obtained with our analytical model (part (a)), and the measured and theoretical results from [22] (part (b)), respectively, for the interior microphone locations 1 and 2, as shown in Fig. 1. Comparing these two figures, it is clear that changing the location of measurement also changes the noise reduction results, as should be expected. To obtain our analytical results, a total number of  $M_x = 10$  and  $M_y = 12$  plate modes, and  $N_x = 3$ ,  $N_y = 4$  and  $N_z = 4$  acoustic modes, was necessary to achieve convergence of the results, for the maximum frequency of interest, i.e., 1000 Hz. It was found that, for the frequency range of interest, [0; 1000] Hz, it is necessary to include some non-resonant modes. A detailed explanation of criterion followed to determine the number of structural modes and acoustic modes required for convergence can be found in [38].

By comparison of parts (a) and (b) of Figs. 2 and 3, it can be concluded that our analytical model provides a good approximation to the experimental data from [22]. Comparing the analytical results in parts (a) and (b), it is clear that results from our framework confirm the existence of a more complex trend line, compared with the analytical results in [22]. This is explained by the fact that, in the present study, a much larger number of plate and acoustic modes were considered, compared with the number of modes used in [22]. An important conclusion from these results is that the number of modes, considered to obtain the analytical results, plays a crucial role in achieving an accurate prediction of the interior noise. However, some differences exist between our analytical results and the experimental results from [22]. As explained in [22], some acoustic leakage through the enclosure sides was observed during experiments, and those differences may be explained due to this factor.

### 7.2 Validation Case 2

The second case chosen for validation of our analytical model is based on the study described in [8]. It consists of a rectangular simply supported aluminum panel, which was flush mounted in the floor of a wind tunnel test section. An acoustically treated enclosure was mounted below the panel.

The sound pressure level, due to the noise radiated from the panel, was measured at various microphone locations inside the acoustic enclosure. Additionally, an accelerometer was located in the centre of the plate to evaluate the vibration levels. A schematic of the physical system is shown in Fig. 4.

The reference power spectral density of the external pressure field is approximately constant, as follows:

$$S_{\text{ref}} = 7.5 \times 10^{-5} \lambda^2 \rho^2 U_{\infty}^3 \delta^*, \quad (34)$$

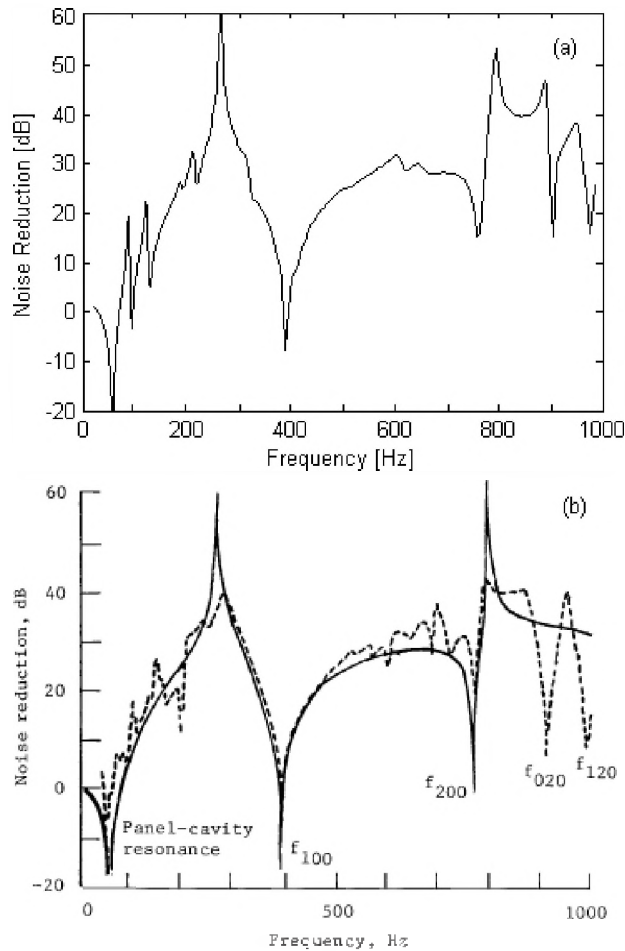


Figure 2. Noise reduction results for validation case 1, obtained for microphone location 1. (a) Obtained using our analytical model. (b) From [22]: —, analytical results; ---, experimental data.

in which  $\lambda = 3$ ,  $\rho$  is the external air density, and  $\delta^*$  is the boundary layer displacement thickness. As explained in [8], a displacement thickness of 12.8 cm gives a correct value for the pressure power spectra, and was used for the calculation of the turbulent excitation. The dimensions and characteristics of the panel and acoustic enclosure, and the properties of the external fluid are displayed in Table 2.

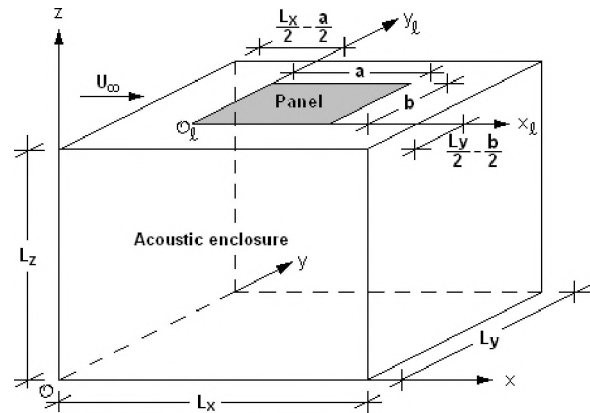


Figure 3. Schematic of physical system of validation case 2.

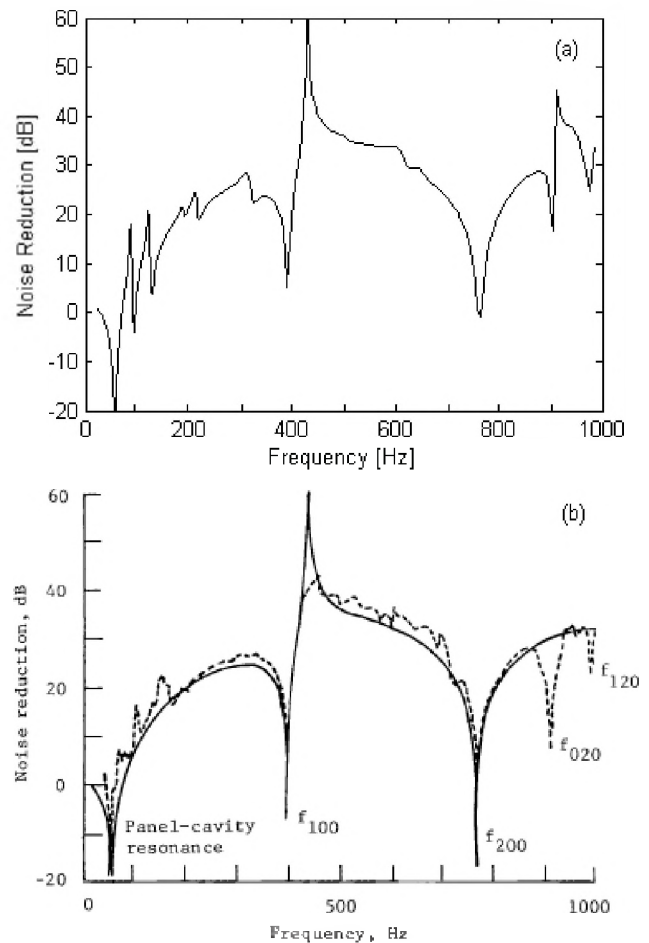


Figure 4. Noise reduction results for validation case 1, obtained for microphone location 2. (a) Obtained using our analytical model. (b) From [22]: —, analytical results; ---, experimental data.

The analytical results obtained using our framework are compared with the results from [8], as shown in Figs. 5 and 6. In Fig. 5, the response at higher frequencies is not accurately predicted by calculations in [8]. Both analytical results in parts (a) and (b) of Fig. 5 overpredict the acceleration level in the region from 900 Hz to 1000 Hz. However, our model is able to accurately predict the acceleration magnitude across the 700-900 Hz region. As

stated in the validation case 1 section, this may be related with the number of structural and acoustic modes considered in the analysis. To accomplish convergence of the spectral quantities, a total number of  $M_x = 5$  and  $M_y = 4$  plate modes, and  $N_x = 8$ ,  $N_y = 6$  and  $N_z = 5$  acoustic modes were used in our model. Again, not only resonant modes were considered in the analyses - a considerable number of non-resonant modes were necessary to achieve convergence of the results. The predicted SPL from our model is shown in Fig. 6 (a). The model accurately predicts the sound pressure levels obtained experimentally in [8], with the main differences observed for low frequencies.

**Table 2. Parameters of the physical system for validation case 2.**

External Flow Properties (Air)		
Variable	Description	Value
$\rho$	Density	1.225 Kg m <sup>-3</sup>
$U_{\square}$	Free stream velocity	35.8 m s <sup>-1</sup>
$U_c$	Convective velocity	0.65 $U_{\square}$
$\alpha_x / \alpha_y$	Empirical parameters	0.115/0.7
Plate Properties (Aluminum)		
Variable	Description	Value
$\rho_p$	Density	2800 Kg m <sup>-3</sup>
$E_p$	Elasticity Modulus	6.5 × 10 <sup>10</sup> Pa <sup>2</sup>
$\nu$	Poisson's ratio	0.3
$\xi_{sp}$	Damping ratio	0.01
$h_p$	Thickness	0.0048 m
$a / b$	Length / Width	0.46 m/0.33 m
Acoustic Enclosure Properties (Air)		
Variable	Description	Value
$c_0$	Speed of sound	340 m s <sup>-1</sup>
$\xi_{ac}$	Damping ratio	0.03
$L_x$	Length	1.05 m
$L_y$	Width	0.857 m
$L_z$	Height	0.635 m

### 7.3 Validation Case 3

The study chosen as the validation case 3, [2], investigates the modeling of an elastic panel coupled with an acoustic enclosure, with the plate occupying a portion of the cavity and subjected to a convected flow, as shown in Fig. 7. The system parameters can be seen in Table 3.

In this study, the model consists of four parts: (1) the external aerodynamic model, (2) the TBL model, (3) the plate model, and (4) the acoustic cavity model. Their model is based on the power balance equation, written in the frequency domain, with the transfer functions of the system of equations computed using MATLAB, and using 4 plate modes and 17 cavity modes (i.e., resonant modes for frequencies up to 1000 Hz). For this frequency range, the TBL point pressure power spectrum was taken to be constant, as follows

$$S_{ref}(\omega_{max}) = 3.84 \times 10^{-5} \frac{(\rho U_{\omega}^2)^2}{4 \omega_{max}}, \quad (35)$$

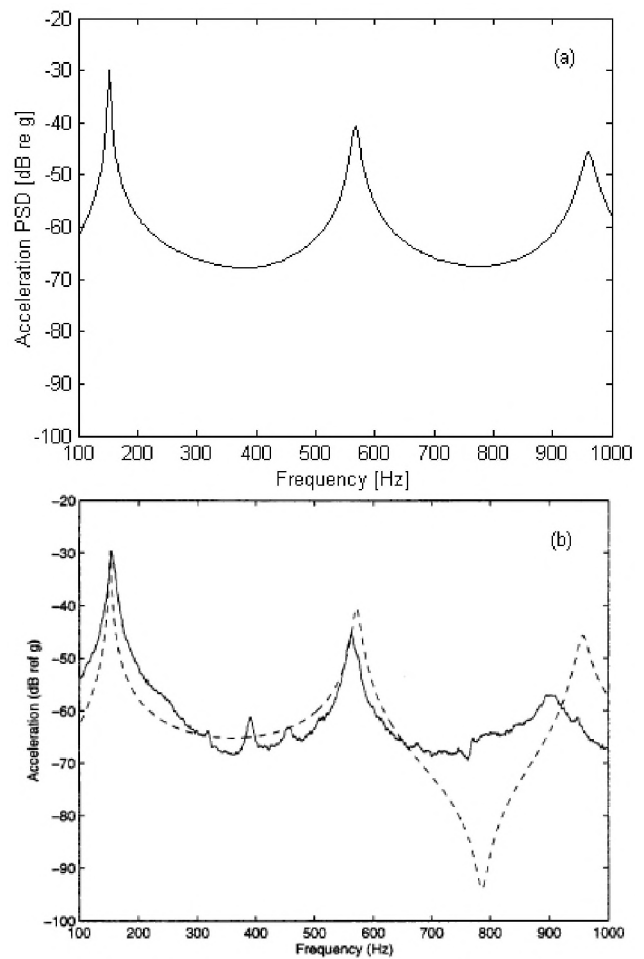


**Figure 5. Validation case 2: acceleration power spectral density. (a) Analytical results obtained using our model. (b) From [8]: ---, calculated; —, measured.**

in which  $\omega_{max}$  is the maximum frequency of interest. Assuming 4 plate modes and 17 cavity modes, the results for the cavity power spectrum are shown in Fig. 8. The cavity power spectrum was calculated through the acoustic pressure PSD,  $S_{pp}(\omega)$ , defined in Eq.(30), as following

$$E_{pp}(\omega) = \frac{L_x L_y L_z}{4 \rho_0 c_0^2} \omega S_{pp}(\omega), \quad (36)$$

Comparing results in parts (a) and (b) of Fig. 8, one can conclude that they in very good agreement, taking into account the entire frequency spectrum. One might now consider a more accurate result as a larger number of plate and cavity modes should be needed in the model. Again, aiming for convergence of calculated spectral quantities, one must consider a total number of  $M_x = 5$  and  $M_y = 5$  plate modes, and  $N_x = 21$ ,  $N_y = 3$  and  $N_z = 3$  acoustic modes in the series expansion. With this number of system natural modes, the results become different, as shown in Fig. 9. As can be concluded by comparison of Figs. 8 and 9, a larger number of modes results in higher cavity power spectrum amplitudes, mainly for frequencies above 300 Hz. The

bigger amount of spectral peaks above 300 Hz displayed in the more accurate results, shown in Fig. 9, is associated with the additional resonant modes considered. Results for lower frequencies remain essentially unaltered from Fig. 8 to Fig. 9.

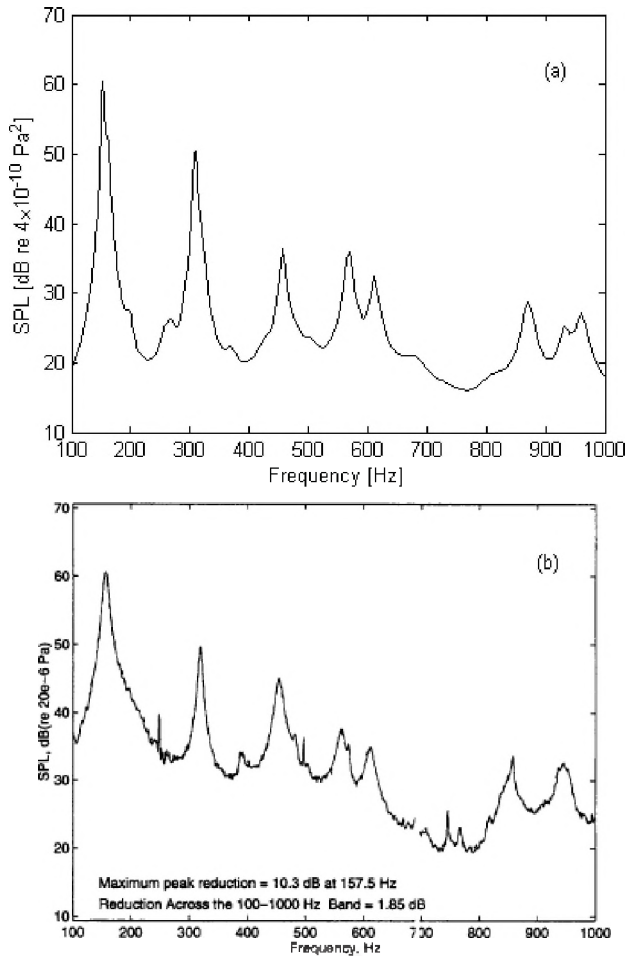


Figure 6. Validation case 2: Sound pressure level: (a) obtained using our analytical model; (b) experimental data from [8].

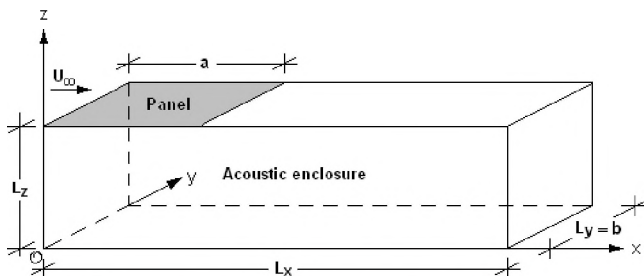


Figure 7. Schematic of the validation case 3 physical system.

Table 3. Properties of the system for the validation case 3.

External Flow Properties (Air)		
Variable	Description	Value
$c_0$	Speed of sound	$310 \text{ m s}^{-1}$
$\rho$	Density	$0.42 \text{ Kg m}^{-3}$
$U_{\infty 1}$	Free stream velocity 1	$0.1 c_0$
$U_{\infty 2}$	Free stream velocity 2	$0.5 c_0$
$U_{\infty 3}$	Free stream velocity 3	$0.8 c_0$

$U_c$	Convective velocity	$0.6 U_{\infty}$
$\alpha_x$	Empirical parameter	0.1
$\alpha_v$	Empirical parameter	0.5

Plate Properties (Aluminum)		
Variable	Description	Value
$\rho_p$	Density	$2800 \text{ Kg m}^{-3}$
$E_p$	Elasticity Modulus	$7.0 \times 10^{10} \text{ Pa}^2$
$\nu$	Poisson's ratio	0.3
$\zeta_{p1}$	Damping ratio 1	0.01
$\zeta_{p2}$	Damping ratio 2	0.02
$\zeta_{p3}$	Damping ratio 3	0.03
$h_p$	Thickness	0.0018 m
$a$	Length	0.3 m
$b$	Width	0.3 m

Acoustic Enclosure Properties (Air)		
Variable	Description	Value
$c_0$	Speed of sound	$310 \text{ m s}^{-1}$
$\rho_0$	Density	$0.42 \text{ Kg m}^{-3}$
$\zeta_{ac}$	Damping ratio	0.05
$L_x$	Length	3.0 m
$L_y$	Width	0.3 m
$L_z$	Height	0.3 m

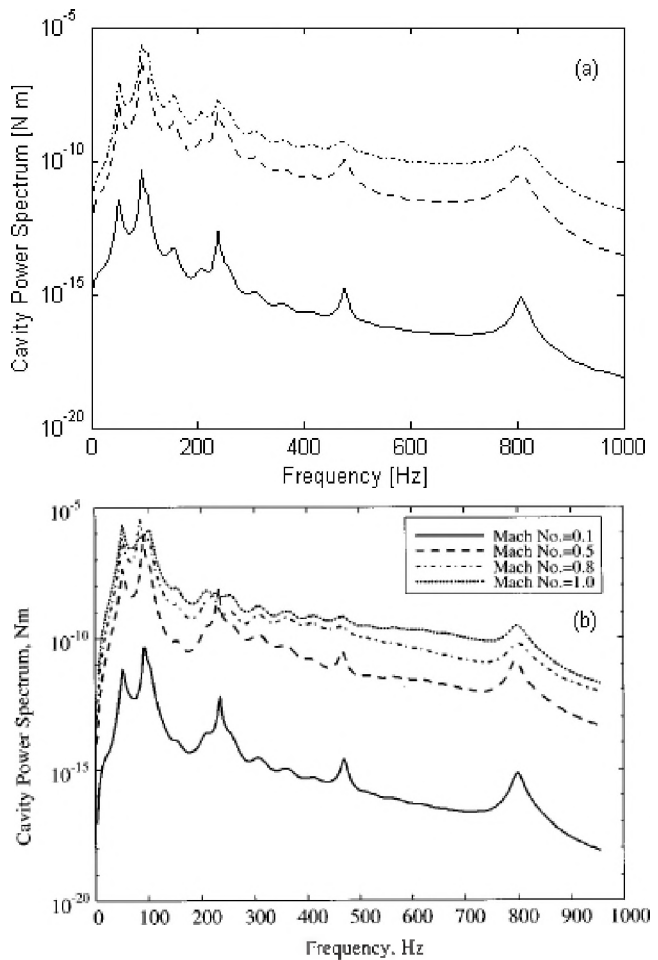


Figure 8. Validation case 3: cavity power spectrum results (using 4 plate modes and 17 cavity modes): —,  $M=0.1$ ; - - -,  $M=0.5$ ; - · - ·,  $M=0.8$ .

(a) From our analytical framework. (b) From [2].

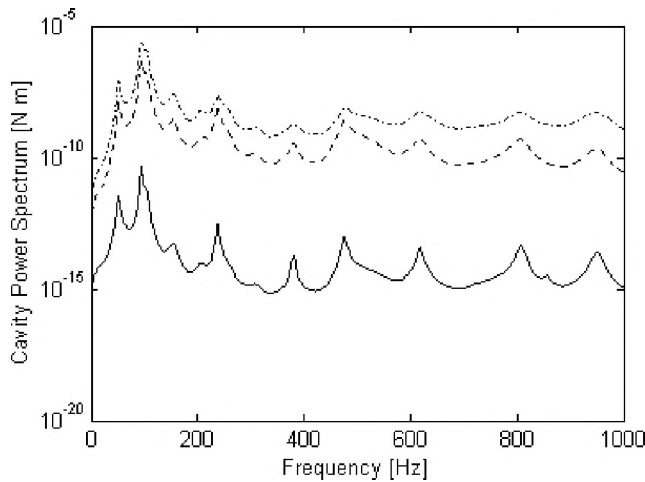


Figure 9. Validation case 3: cavity power spectrum results from our analytical framework (using a larger number of plate and cavity modes): —,  $M=0.1$ ; ---,  $M=0.5$ ; - · - ·,  $M=0.8$ .

#### 7.4 Validation Case 4

The validation case 4 is the study by [37]. As in the previous validation case, this study investigates the model of a convected fluid loaded plate coupled with an acoustic enclosure. However, the dimensions are different from the previous case, and were chosen to reproduce a small commercial aircraft. The physical system schematic is shown in Fig. 10 and the main parameters of the system are displayed in Table 4.

Table 4. System parameter of validation case 4.

External Flow Properties (Air)		
Variable	Description	Value
$c_0$	Speed of sound	$310 \text{ m s}^{-1}$
$\rho$	Density	$0.42 \text{ Kg m}^{-3}$
$U_\infty$	Free stream velocity	$0.1 c_0$
$U_c$	Convective velocity	$0.6 U_\infty$
$\alpha_x$	Empirical parameter	0.1
$\alpha_y$	Empirical parameter	0.5
Plate Properties (Aluminum)		
Variable	Description	Value
$\rho_p$	Density	$2700 \text{ Kg m}^{-3}$
$E_p$	Elasticity Modulus	$7.1 \times 10^{10} \text{ Pa}^2$
$\nu$	Poisson's ratio	0.3
$\xi_{sp}$	Damping ratio	0.01
$h_p$	Thickness	0.0022 m
$a$	Length	0.6 m
$b$	Width	0.525 m
$x_p$	Plate x-coordinate	0.6 m
$y_p$	Plate y-coordinate	0.6 m
Acoustic Enclosure Properties (Air)		
Variable	Description	Value
$c_0$	Speed of sound	$310 \text{ m s}^{-1}$
$\rho_0$	Density	$0.42 \text{ Kg m}^{-3}$
$\xi_{ac}$	Damping ratio	0.05
$L_x$	Length	6.0 m
$L_y$	Width	1.8 m
$L_z$	Height	1.8 m

In [37], a total number of 50 acoustic modes and 20 plate modes were used to obtain the numerical results. For this number of natural modes, the results for the cavity acoustic potential energy are shown in Fig. 11. Fig. 12 shows the

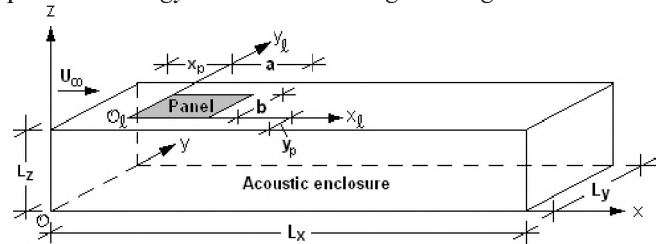


Figure 10. Physical system of validation case 4.

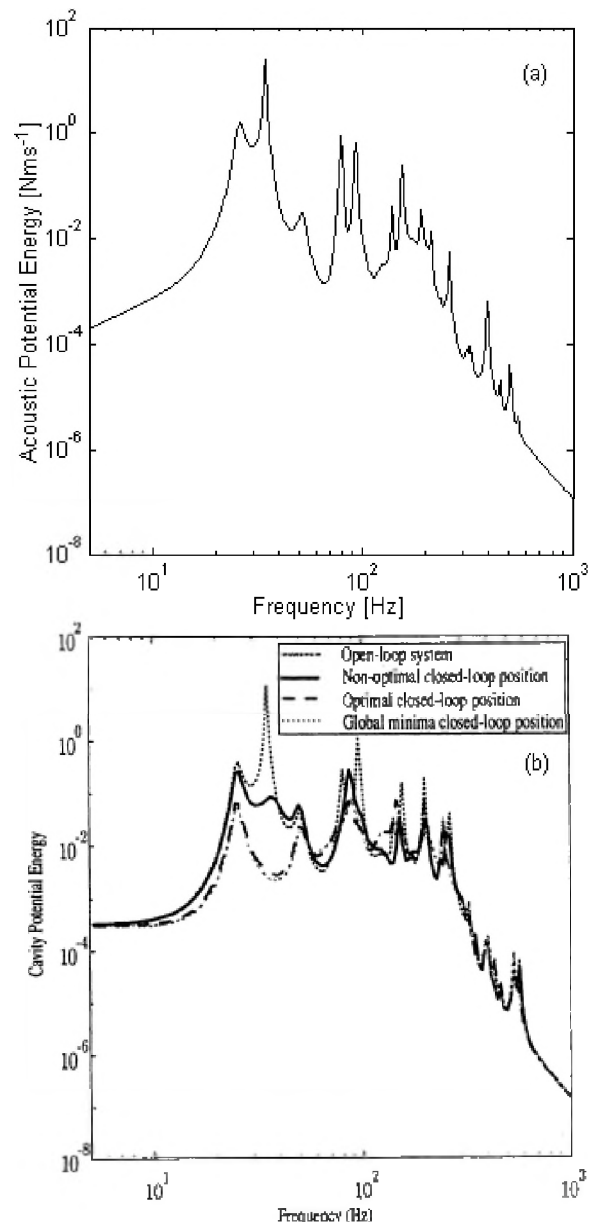


Figure 11. Validation case 4: acoustic potential energy results (using 20 plate modes and 50 cavity modes): (a) obtained using our analytical framework; (b) from [37].

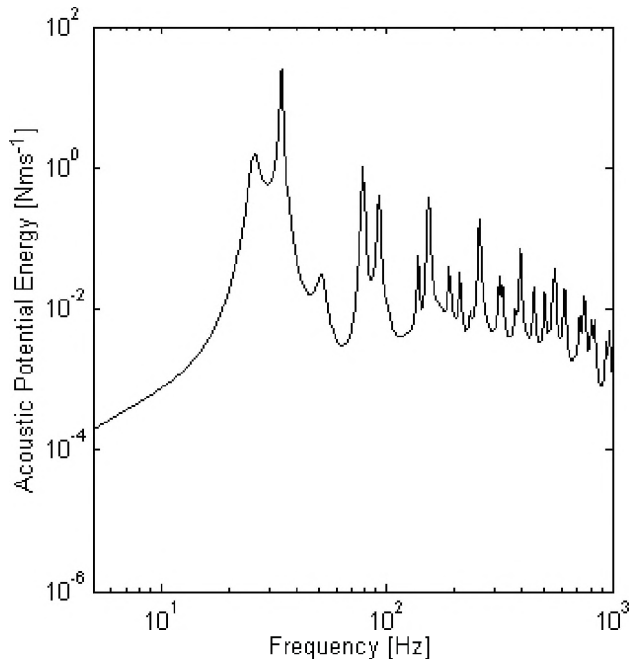


Figure 12. Validation case 4: acoustic potential energy results from our analytical framework (using a larger number of plate and acoustic modes).

results obtained with analytical results, but using a total number of  $M_x = 9$  and  $M_y = 7$  plate modes, and  $N_x = 40$ ,  $N_y = 7$  and  $N_z = 7$  acoustic modes, in order to obtain accurate results in the bandwidth of interest. To calculate the cavity potential energy, in Figs. 11 and 12, the following equation was used

$$E_{pp}(\omega) = \frac{L_x L_y L_z}{4 \rho_0 c_0^2} \omega^2 S_{pp}(\omega), \quad (37)$$

in which  $S_{pp}(\omega)$  is defined by Eq.(30). Comparing parts (a) and open-loop plot in part (b) of Fig. 11, one can conclude that results are in good agreement. However, when considering a larger number of natural modes, the results are very different, mainly for higher frequencies, as shown in Fig. 12. The consideration of the larger number of system modes results in an increase of acoustic energy for frequencies above 200 Hz.

## 8. CONCLUSIONS

The model validation is an essential part of the model development process in order to the models to be accepted and used as a predictive tool. Several independent experimental and numerical studies, with different physical properties and environment, were used for conducting the validation of our model. The analytical results from our model show an overall match with the data from the validation cases. This indicates that our model can be used for the prediction of noise levels, and applicable for different practical cases.

The analytical model has applied for the prediction of noise levels to 4 different cases. The analytical predictions of the plate vibration PSD and the enclosure pressure PSD were calculated in order to perform the comparative analysis with the experimental and numerical data from the validation cases. In all 4 analyses, the predicted values are in good agreement with the data from the validation chosen studies. Additionally, it was found that the number of plate and acoustic natural modes used in the analysis play an important role in the model accurate prediction. In fact, there is a minimum number of natural modes which needs to be used in the analysis, in order to accurately predict the noise and vibration levels up to a maximum frequency.

The analytical framework developed and here validated can be used for the noise and vibration levels prediction for physical systems with a rectangular shaped enclosure with one flexible wall. This framework presents a solid basis for further analyses, opening the doors for its use in the design and implementation of noise reduction techniques. As demonstrated, accurate analytical models can be used to solve the problem of cabin TBL-induced interior noise prediction. Moreover, being the cabin an acoustic enclosure, it is important to consider not only the structural natural modes associated with the structural panels, but also the cabin acoustic modes, as well. Even though the structural-acoustic coupling turns the analytical framework more complex, it can be a first alternative to the much more time consuming numerical solutions. Future work of the present research will aim for the prediction of TBL-induced noise into an acoustic enclosure with several flexible panels, and also the development of additional analytical frameworks for cylindrical and spherical acoustic enclosures.

## REFERENCES

- [1] D. E. Bishop, Cruise flight noise levels in a turbojet transport airplane. *Noise Control* (1961), 7, pp. 37-42.
- [2] K. D. Frampton and R. L. Clark, Power flow in an aeroelastic plate backed by a reverberant cavity. *Journal of the Acoustical Society of America* (1997), 102(3), pp. 1620-1627.
- [3] W. V. Bhat, Flight test measurement of measurement of exterior turbulent boundary layer pressure fluctuations on Boeing Model 737 airplane. *Journal of Sound and Vibration* (1971), 14 (4), pp. 439-457.
- [4] W. V. Bhat and J. F. Wilby, Interior noise radiated by an airplane fuselage subjected to turbulent boundary layer excitation and evaluation of noise reduction treatments. *Journal of Sound and Vibration* (1971), 18 (4), pp. 449-464.
- [5] G. P. Gibbs, R. H. Cabell and J. Juang, Controller Complexity for Active Control of Turbulent Boundary-Layer Noise from Panels. *AIAA Journal* (2004), 42(7), pp. 1314-1320.
- [6] A. Bullmore, P. Nelson, and S. Elliot. Theoretical studies of the active control of propeller-induced cabin noise. *Journal of Sound and Vibration* (1990), 140(2), pp. 191-217.

- [7] D. MacMartin. Collocated structural control for reduction of aircraft cabin noise. *Journal of Sound and Vibration* (1996), 190(1), pp. 105-119.
- [8] C. M. Heatwole, R. J. Bernhard and M. A. Francheck, Robust feedback control of flow induced structural radiation of sound. *NASA Report 0278-1* (1997).
- [9] J. Henry and R. Clark. Active control of sound transmission through a curved panel into a cylindrical enclosure. *Journal of Sound and Vibration* (2002), 249(2), pp. 325-349.
- [10] D. A. Bies, A review of flight and wind tunnel measurements of boundary layer pressure fluctuations and induced structural response, *NASA CR-626* (1966).
- [11] L. Maestrello, Measurement of noise radiated by turbulent boundary layer excited panels. *Journal of Sound and Vibration* (1965), 2(2), pp. 100-115.
- [12] L. Maestrello, Radiation from and panel response to a supersonic turbulent boundary layer. *Journal of Sound and Vibration* (1969), 10(2), pp. 261-295.
- [13] J. F. Wilby and F. L. Gloyna, Vibration measurements of an airplane fuselage structure I. Turbulent boundary layer excitation. *Journal of Sound and Vibration* (1972), 23, pp. 443-466.
- [14] J. F. Wilby and F. L. Gloyna, Vibration measurements of an airplane fuselage structure II. Jet noise excitation. *Journal of Sound and Vibration* (1972), 23 (4), pp. 467-486.
- [15] J. F. Wilby, Aircraft interior noise. *Journal of Sound and Vibration* (1996), 190 (3), pp. 545-564.
- [16] W. A. Strawderman, Turbulent-flow-excited vibration of a simply supported, rectangular flat plate. *The Journal of the Acoustical Society of America* (1969), 45(1), pp. 177-192.
- [17] H. G. Davies, Sound from turbulent boundary layer excited panels. *The Journal of the Acoustical Society of America* (1971), 55, pp. 213-219.
- [18] R. L. Clark and K. Frampton, Aeroelastic structural acoustic coupling: implications on the control of turbulent boundary-layer noise transmission. *Journal of the Acoustical Society of America* (1997), 102(3), pp. 1639-1647.
- [19] C. Maury, P. Gardonio and S.J. Elliot, A wavenumber approach to the modeling the response of a random excited panel, Part II: application to aircraft panels excited by a turbulent boundary layer. *Journal of Sound and Vibration* (2002), 252(1), pp. 115-139.
- [20] J. Park, T. Siegmund and L. Mongeau, Analysis of the flow-induced vibration of viscoelastically supported rectangular plates. *Journal of Sound and Vibration* (2003), 261, pp. 225-245.
- [21] R. Vaicaitis and M. Slazak, Noise transmission through stiffened panels. *Journal of Sound and Vibration* (1980), 70(3), pp. 413-426.
- [22] C. K. Barton and E. F. Daniels, Noise transmission through flat rectangular panels into a closed cavity, *NASA TP-1321* (1978).
- [23] G. Corcos, The structure of the turbulent pressure field in boundary layer flows. *Journal of Fluid Mechanics - Cambridge Journal Online* (1964), 18, pp. 353-378.
- [24] G. Corcos, Resolution of pressure in turbulence. *Journal of the Acoustical Society of America* (1963), 35(2), pp. 192-199.
- [25] B. M. Efimtsov, Characteristics of the field of turbulent wall pressure fluctuations at large Reynolds numbers. *Soviet Physics-Acoustics* (1982), 28 (4), pp. 289-292.
- [26] D. M. Chase, Modelling the wavevector-frequency spectrum of turbulent boundary layer wall-pressure. *Journal of Sound and Vibration* (1980), 70, pp. 29-67.
- [27] D. M. Chase, The character of the turbulent wall pressure spectrum at subconvective wavenumbers and a suggested comprehensive model. *Journal of Sound and Vibration* (1987), 112, pp. 125-147.
- [28] J. E. Ffowcs Williams, Boundary-layer pressures and the Corcos model: a development to incorporate lowwavenumber constraints. *Journal of Fluid Mechanics* (1982), 125, pp. 9-25.
- [29] A. V. Smol'yakov and V. M. Tkachenko, Model of a field of pseudonic turbulent wall pressures and experimental data. *Soviet Physics-Acoustics* (1991), 37 (6), pp. 627-631.
- [30] C. Maury, P. Gardonio and S. J. Elliot, Active control of the flow-induced noise transmitted through a panel. *AIAA Journal* (2001), 39(10), pp. 1860-1867.
- [31] D. R. Thomas and P. A. Nelson, Feedback control of sound radiation from a plate excited by a turbulent boundary layer. *Journal of the Acoustical Society of America* (1995), 98(5), pp. 2651-2662.
- [32] F. Han, L. G. Mongeau and R. J. Bernhard, A model for the vibro-acoustic response of plates excited by complex flows. *Journal of Sound and Vibration* (2001), 246(5), pp. 901-926.
- [33] C. Maury, P. Gardonio and S. J. Elliot, Model for the active control of flow-induced noise transmitted through double partitions. *AIAA Journal* (2002), 40(6), pp. 1113-1121.
- [34] C. Maury, P. Gardonio and S. J. Elliot, A wavenumber approach to modeling the response of a randomly excited panel, part I: general theory. *Journal of Sound and Vibration* (2002), 252(1), pp. 83-113.
- [35] S. J. Elliot, C. Maury and P. Gardonio, The synthesis of spatially correlated random pressure fields. *Journal of the Acoustical Society of America* (2005), 117(3), pp. 1186-1201.
- [36] J. Rohlffing and P. Gardonio, Active Control of Sound Transmission through Panels with Flexible Boundaries under Deterministic and Stochastic Excitation, *Institute of Sound and Vibration Research (ISVR) Technical Memorandum 977* (2007), University of Southampton, England.
- [37] G. C. Smith, R. L. Clark and K. D. Frampton. Optimal Transducer Placement for Active Control of Sound Transmission through Aeroelastic Plates. *Journal of the Intelligent Material Systems and Structures* (1998), 9, pp. 975-987.

[38] J. da Rocha, A. Suleman and F. Lau. Structural-acoustic coupling of a multi-panel walled enclosure excited by turbulent flow: contribution of each panel, *Journal of the Acoustical Society of America* (submitted 2009).

[39] W. R. Graham, A comparison of models for the wavenumber frequency spectrum of turbulent boundary layer pressures. *Journal of Sound and Vibration* (1997), 206(4), pp. 541-565.

[40] R. Rackl and A. Weston, Modeling of turbulent boundary layer surface pressure fluctuation auto and cross spectra - verification and adjustments based on TU-144LL data, *NASA CR-213938* (2005).

[41] F. Fahy, *Sound and Structural Vibration, Radiation, Transmission and Response*, Academic Press Ltd., London, 1985.

[42] J. Blevins, *Formulas for Natural Frequency and Mode Shape*, Krieger Publishing Company, Malabar, Florida, 2001.

[43] F. Fahy, *Sound and Structural Vibration, Radiation, Transmission and Response*, Academic Press Ltd., London, 1985.

[44] J. Blevins, *Formulas for Natural Frequency and Mode Shape*, Krieger Publishing Company, Malabar, Florida, 2001.

[45] H. Kuttruff, *Room Acoustics*, Applied Science Publishers Ltd., London, 1973.

[46] P. A. Nelson and S. J. Elliot, *Active Control of Sound*, Academic Press Ltd., London, 1992.

[47] D. E. Newland, *An introduction to Random Vibration and Spectral Analysis*, Longman, New York, 1984.

[48] Y. K. Lin, *Probabilistic Theory of Structural Dynamics*, McGraw-Hill Book Company, New York, 1967.

## ACKNOWLEDGEMENTS

The authors would like to thank Zonta International for the financial support to this research, through the Amelia Earhart Fellowship Program.

## APPENDICES

### A. Analytical expressions for $\mathbf{M}_{cp}$ and $\mathbf{K}_{pc}$ matrices

Matrices  $\mathbf{M}_{cp}$  and  $\mathbf{K}_{pc}$  are defined, respectively, by Eqs.(19b) and (19e). To derive the final analytical expressions for these matrices, the integrals over  $x_p$  and  $y_p$  on the equations need to be analytically obtained. Starting by the derivation of the mass matrix,  $\mathbf{M}_{cp}$ , by substituting Eqs. (6) and (10) into Eq.(19b), it becomes

$$\mathbf{M}_{cp} = \frac{2 \rho_0}{\sqrt{a b L_x L_y L_z}} \left[ (-1)^{n_z} A_{n_x} A_{n_y} A_{n_z} \int_{x_{p_i}}^{x_{p_f}} \sin\left(\frac{m_x \pi (x - x_{p_i})}{a}\right) \right]$$

$$\cos\left(\frac{n_x \pi x}{L_x}\right) dx \int_{y_{p_i}}^{y_{p_f}} \sin\left(\frac{m_y \pi (y - y_{p_i})}{b}\right) \cos\left(\frac{n_y \pi y}{L_y}\right) dy, \quad (\text{A.1})$$

where  $x$  and  $y$  correspond to the acoustic enclosure (global coordinate system, and terms inside [ ] are developed to obtain a matrix, according with the  $n$  and  $m$  indexes. Note that, in Eq. (A.1), the plate spatial functions, defined in Eqs. (6a) and (6b), were modified in order to be expressed in the enclosure coordinate system. For convenience, one may consider Eq.(A.1) written as the an alternative form as

$$\mathbf{M}_{cp} = \frac{2 \rho_0}{\sqrt{a b L_x L_y L_z}} \left[ (-1)^{n_z} A_{n_x} A_{n_y} A_{n_z} B_{nm}(x) B_{nm}(y) \right], \quad (\text{A.2})$$

with:

$$B_{nm}(x) = \int_{x_{p_i}}^{x_{p_f}} \sin\left(\frac{m_x \pi (x - x_{p_i})}{a}\right) \cos\left(\frac{n_x \pi x}{L_x}\right) dx, \quad (\text{A.3a})$$

$$B_{nm}(y) = \int_{y_{p_i}}^{y_{p_f}} \sin\left(\frac{m_y \pi (y - y_{p_i})}{b}\right) \cos\left(\frac{n_y \pi y}{L_y}\right) dy. \quad (\text{A.3b})$$

The analytical development of the functions  $B_{nm}(x)$  and  $B_{nm}(y)$  results in the following final expressions:

$$B_{nm}(x) = \begin{cases} f(x_{p_f}) - f(x_{p_i}), & \left(\frac{m_x}{a} \neq \frac{n_x}{L_x}\right) \wedge \left(\frac{x_{p_i}}{a} \text{ even}\right) \\ f(x_{p_f}) - f(x_{p_i}), & \left(\frac{m_x}{a} \neq \frac{n_x}{L_x}\right) \wedge \left(\frac{x_{p_i}}{a} \text{ odd}\right) \wedge (m_x \text{ even}) \\ f(x_{p_i}) - f(x_{p_f}), & \left(\frac{m_x}{a} \neq \frac{n_x}{L_x}\right) \wedge \left(\frac{x_{p_i}}{a} \text{ odd}\right) \wedge (m_x \text{ odd}) \\ 0, & \left(\frac{m_x}{a} = \frac{n_x}{L_x}\right) \end{cases} \quad (\text{A.4a})$$

and

$$B_{nm}(y) = \begin{cases} g(y_{p_f}) - g(y_{p_i}), & \left(\frac{m_y}{b} \neq \frac{n_y}{L_y}\right) \wedge \left(\frac{y_{p_i}}{b} \text{ even}\right) \\ g(y_{p_f}) - g(y_{p_i}), & \left(\frac{m_y}{b} \neq \frac{n_y}{L_y}\right) \wedge \left(\frac{y_{p_i}}{b} \text{ odd}\right) \wedge (m_y \text{ even}) \\ g(y_{p_i}) - g(y_{p_f}), & \left(\frac{m_y}{b} \neq \frac{n_y}{L_y}\right) \wedge \left(\frac{y_{p_i}}{b} \text{ odd}\right) \wedge (m_y \text{ odd}) \\ 0, & \left(\frac{m_y}{b} = \frac{n_y}{L_y}\right) \end{cases} \quad (\text{A.4b})$$

in which:

$$f(x) = \frac{\cos\left[\left(\frac{m_x}{a} + \frac{n_x}{L_x}\right) \pi x\right]}{2\left(\frac{m_x}{a} + \frac{n_x}{L_x}\right) \pi} + \frac{\cos\left[\left(\frac{m_x}{a} - \frac{n_x}{L_x}\right) \pi x\right]}{2\left(\frac{m_x}{a} - \frac{n_x}{L_x}\right) \pi}, \quad (\text{A.5a})$$

and

$$g(y) = \frac{\cos\left[\left(\frac{m_y}{b} + \frac{n_y}{L_y}\right)\pi y\right]}{2\left(\frac{m_y}{b} + \frac{n_y}{L_y}\right)\pi} + \frac{\cos\left[\left(\frac{m_y}{b} - \frac{n_y}{L_y}\right)\pi y\right]}{2\left(\frac{m_y}{b} - \frac{n_y}{L_y}\right)\pi}, \quad (\text{A.5b})$$

Similarly to mass matrix, the stiffness matrix,  $\mathbf{K}_{pc}$ , may be written in the following form

$$\mathbf{K}_{cp} = -\frac{2}{\sqrt{a b L_x L_y L_z}} \left[ (-1)^{n_z} A_{n_x} A_{n_y} A_{n_z} B_{mn}(x) B_{mn}(y) \right], \quad (\text{A.6})$$

with functions  $B_{mn}(x)$  and  $B_{mn}(y)$  defined by Eqs.(A.4a) and (A.4b), respectively.

## B. Analytical expression derived for $S_{tbl}(\omega)$ matrix

Substituting Eqs.(4) and (6) into Eq.(28),  $S_{tbl}(\omega)$  matrix becomes defined as follows

$$S_{tbl}(\omega) = \frac{4 S_{ref}(\omega)}{a b} \left[ \int_{x_{p1}}^{x_{pf}} \int_{y_{p1}}^{y_{pf}} \sin\left(\frac{m_x \pi x}{a}\right) \sin\left(\frac{m'_x \pi x'}{a}\right) e^{-\frac{\alpha_x \omega |x-x'|}{U_c}} e^{-\frac{i \omega (x-x')}{U_c}} dx dx' \int_{y_{p1}}^{y_{pf}} \sin\left(\frac{m_y \pi y}{b}\right) \sin\left(\frac{m'_y \pi y'}{b}\right) e^{-\frac{\alpha_y \omega |y-y'|}{U_c}} dy dy' \right] \quad (\text{B.1})$$

in which terms inside [ ] are developed to obtain a matrix, according with the  $m$  and  $m'$  indexes, and  $x$  and  $y$  correspond to plate (local) coordinate system. After some mathematical manipulation, Eq. (B.1) can be written as

$$S_{tbl}(\omega) = \frac{4 S_{ref}(\omega)}{a b} \left[ \int_{x_{p1}}^{x_{pf}} \sin\left(\frac{m'_x \pi x'}{a}\right) \left\{ e^{-\frac{x'(-\alpha_x+i)\omega}{U_c}} \int_{x_{p1}}^{x'} \sin\left(\frac{m_x \pi x}{a}\right) e^{-\frac{x(-\alpha_x-1)\omega}{U_c}} dx + e^{-\frac{x(\alpha_x-1)\omega}{U_c}} \int_{x'}^{x_{pf}} \sin\left(\frac{m_x \pi x}{a}\right) e^{-\frac{x(-\alpha_x-1)\omega}{U_c}} dx \right\} dx' \int_{y_{p1}}^{y_{pf}} \sin\left(\frac{m_y \pi y'}{b}\right) \left\{ e^{-\frac{y' \alpha_y \omega}{U_c}} \int_{y_{p1}}^{y'} \sin\left(\frac{m_y \pi y}{b}\right) e^{-\frac{y \alpha_y \omega}{U_c}} dy + e^{-\frac{y' \alpha_y \omega}{U_c}} \int_{y'}^{y_{pf}} \sin\left(\frac{m_y \pi y}{b}\right) e^{-\frac{y \alpha_y \omega}{U_c}} dy \right\} dy' \right], \quad (\text{B.2})$$

Developing Eq.(B.2) analytically, one obtains the final analytical expression for the  $S_{tbl}(\omega)$  matrix components, which become defined as follows:

$$S_{tbl}(\omega)_{m, m'} = \frac{4 S_{ref}(\omega)}{a b} \left\{ [C_{x1}(\omega, m) C_{x5}(m, m') + C_{x2}(\omega, m) C_{x6}(m, m') + C_{x3}(\omega, m) C_{x7}(\omega, m') + C_{x4}(\omega, m) C_{x8}(\omega, m')] \right\}$$

$$[C_{y1}(\omega, m) C_{y5}(m, m') + C_{y3}(\omega, m) C_{y7}(\omega, m') + C_{y4}(\omega, m) C_{y8}(\omega, m')], \quad (\text{B.3})$$

in which functions  $C$ 's are defined by the following analytical expressions:

$$C_{x1}(\omega, m) = \frac{2\alpha_x \omega}{U_c} \frac{\left(\frac{\omega}{U_c}\right)^2 (\alpha_x^2+1) + \left(\frac{m_x \pi}{a}\right)^2}{\left[\left(\frac{\omega}{U_c}\right)^2 (\alpha_x^2-1) + \left(\frac{m_x \pi}{a}\right)^2\right]^2 + \left[2\alpha_x \left(\frac{\omega}{U_c}\right)^2\right]^2}, \quad (\text{B.4})$$

$$C_{x2}(\omega, m) = -\frac{\left(\frac{m_x \pi}{a}\right) \left(\frac{4\alpha_x \omega^2}{U_c}\right) i}{\left[\left(\frac{\omega}{U_c}\right)^2 (\alpha_x^2-1) + \left(\frac{m_x \pi}{a}\right)^2\right]^2 + \left[2\alpha_x \left(\frac{\omega}{U_c}\right)^2\right]^2}, \quad (\text{B.5})$$

$$C_{x3}(\omega, m) = -\frac{e^{-\frac{x_{p1}(\alpha_x-1)\omega}{U_c}}}{\left[\left(\frac{\omega}{U_c}\right)^2 (\alpha_x^2-1) + \left(\frac{m_x \pi}{a}\right)^2\right]^2 + \left[2\alpha_x \left(\frac{\omega}{U_c}\right)^2\right]^2} \left\{ \left[\left(\frac{\omega}{U_c}\right)^2 (\alpha_x^2-1) + \left(\frac{m_x \pi}{a}\right)^2\right] + 2\alpha_x \left(\frac{\omega}{U_c}\right)^2 i \right\} \left[ \frac{(\alpha_x-i)\omega}{U_c} \sin\left(\frac{m_x \pi x_{p1}}{a}\right) - \frac{m_x \pi}{a} \cos\left(\frac{m_x \pi x_{p1}}{a}\right) \right], \quad (\text{B.6})$$

$$C_{x4}(\omega, m) = -\frac{e^{-\frac{(x_{p1}+a)(\alpha_x+i)\omega}{U_c}} \cos(m_x \pi)}{\left[\left(\frac{\omega}{U_c}\right)^2 (\alpha_x^2-1) + \left(\frac{m_x \pi}{a}\right)^2\right]^2 + \left[2\alpha_x \left(\frac{\omega}{U_c}\right)^2\right]^2} \left\{ \left[\left(\frac{\omega}{U_c}\right)^2 (\alpha_x^2-1) + \left(\frac{m_x \pi}{a}\right)^2\right] - 2\alpha_x \left(\frac{\omega}{U_c}\right)^2 i \right\} \left[ \frac{(\alpha_x+i)\omega}{U_c} \sin\left(\frac{m_x \pi x_{p1}}{a}\right) + \frac{m_x \pi}{a} \cos\left(\frac{m_x \pi x_{p1}}{a}\right) \right], \quad (\text{B.7})$$

$$C_{x5}(m, m') = \begin{cases} \frac{a}{2}, & \text{for } m_x = m'_x \\ \text{Const.}_{x5}, & \text{for } m_x \neq m'_x \end{cases} \quad (\text{B.8a})$$

with:

$$\text{Const.}_{x5} = \frac{-\sin\left[(m'_x + m_x) \frac{\pi}{a} (x_{p1} + a)\right] + \sin\left[(m'_x + m_x) \frac{\pi}{a} x_{p1}\right]}{2(m'_x + m_x) \frac{\pi}{a}} + \frac{\sin\left[(m'_x - m_x) \frac{\pi}{a} (x_{p1} + a)\right] - \sin\left[(m'_x - m_x) \frac{\pi}{a} x_{p1}\right]}{2(m'_x - m_x) \frac{\pi}{a}}, \quad (\text{B.8b})$$

$$C_{x6}(m, m') = \begin{cases} 0, & \text{for } m_x = m'_x \\ \text{Const.}_{x6}, & \text{for } m_x \neq m'_x \end{cases} \quad (\text{B.9a})$$

$$\text{Const.}_{x_6} = \frac{-\cos\left[(m'_x + m_x)\frac{\pi}{a}(x_{p_1} + a)\right] + \cos\left[(m'_x + m_x)\frac{\pi}{a}x_{p_1}\right]}{2(m'_x + m_x)\frac{\pi}{a}} + \frac{-\cos\left[(m'_x - m_x)\frac{\pi}{a}(x_{p_1} + a)\right] + \cos\left[(m'_x - m_x)\frac{\pi}{a}x_{p_1}\right]}{2(m'_x - m_x)\frac{\pi}{a}}, \quad (\text{B.9b})$$

$$C_{x_7}(\omega, m') = \frac{e^{\frac{(x_{p_1} + a)(-\alpha_x + i)\omega}{U_c}}}{\left[\frac{(-\alpha_x + i)\omega}{U_c}\right]^2 + \left(\frac{m'_x\pi}{a}\right)^2} \left\{ \frac{(-\alpha_x + i)\omega}{U_c} \sin\left[\frac{m'_x\pi(x_{p_1} + a)}{a}\right] - \frac{m'_x\pi}{a} \cos\left[\frac{m'_x\pi(x_{p_1} + a)}{a}\right] \right\} - \frac{e^{\frac{x_{p_1}(-\alpha_x + i)\omega}{U_c}}}{\left[\frac{(-\alpha_x + i)\omega}{U_c}\right]^2 + \left(\frac{m'_x\pi}{a}\right)^2} \left\{ \frac{(-\alpha_x + i)\omega}{U_c} \sin\left(\frac{m'_x\pi x_{p_1}}{a}\right) - \frac{m'_x\pi}{a} \cos\left(\frac{m'_x\pi x_{p_1}}{a}\right) \right\}, \quad (\text{B.10})$$

$$C_{x_8}(\omega, m') = \frac{e^{\frac{(x_{p_1} + a)(\alpha_x + i)\omega}{U_c}}}{\left[\frac{(\alpha_x + i)\omega}{U_c}\right]^2 + \left(\frac{m'_x\pi}{a}\right)^2} \left\{ \frac{(\alpha_x + i)\omega}{U_c} \sin\left[\frac{m'_x\pi(x_{p_1} + a)}{a}\right] - \frac{m'_x\pi}{a} \cos\left[\frac{m'_x\pi(x_{p_1} + a)}{a}\right] \right\} - \frac{e^{\frac{x_{p_1}(\alpha_x + i)\omega}{U_c}}}{\left[\frac{(\alpha_x + i)\omega}{U_c}\right]^2 + \left(\frac{m'_x\pi}{a}\right)^2} \left\{ \frac{(\alpha_x + i)\omega}{U_c} \sin\left(\frac{m'_x\pi x_{p_1}}{a}\right) - \frac{m'_x\pi}{a} \cos\left(\frac{m'_x\pi x_{p_1}}{a}\right) \right\}, \quad (\text{B.11})$$

and

$$C_{y_1}(\omega, m) = \frac{2\alpha_y\omega}{U_c} \frac{1}{\left(\frac{\alpha_y\omega}{U_c}\right)^2 + \left(\frac{m_y\pi}{b}\right)^2}, \quad (\text{B.12})$$

$$C_{y_3}(\omega, m) = -\frac{e^{\frac{y_{p_1}\alpha_y\omega}{U_c}}}{\left(\frac{\alpha_y\omega}{U_c}\right)^2 + \left(\frac{m_y\pi}{b}\right)^2} \left[ \frac{\alpha_y\omega}{U_c} \sin\left(\frac{m_y\pi y_{p_1}}{b}\right) - \frac{m_y\pi}{b} \cos\left(\frac{m_y\pi y_{p_1}}{b}\right) \right], \quad (\text{B.13})$$

$$C_{y_4}(\omega, m) = -\frac{e^{-\frac{(y_{p_1} + b)\alpha_y\omega}{U_c}}}{\left(\frac{\alpha_y\omega}{U_c}\right)^2 + \left(\frac{m_y\pi}{b}\right)^2} \left[ \frac{\alpha_y\omega}{U_c} \sin\left(\frac{m_y\pi(y_{p_1} + b)}{b}\right) + \frac{m_y\pi}{b} \cos\left(\frac{m_y\pi(y_{p_1} + b)}{b}\right) \right], \quad (\text{B.14})$$

$$C_{y_5}(m, m') = \begin{cases} \frac{b}{2}, & \text{for } m_y = m'_y \\ \text{Const.}_{y_5}, & \text{for } m_y \neq m'_y \end{cases} \quad (\text{B.15a})$$

with:

$$\text{Const.}_{y_5} = \frac{-\sin\left[(m'_y + m_y)\frac{\pi}{b}(y_{p_1} + b)\right] + \sin\left[(m'_y + m_y)\frac{\pi}{b}y_{p_1}\right]}{2(m'_y + m_y)\frac{\pi}{b}} + \frac{\sin\left[(m'_y - m_y)\frac{\pi}{b}(y_{p_1} + b)\right] - \sin\left[(m'_y - m_y)\frac{\pi}{b}y_{p_1}\right]}{2(m'_y - m_y)\frac{\pi}{b}}, \quad (\text{B.15b})$$

$$C_{y_7}(\omega, m') = \frac{e^{-\frac{(y_{p_1} + b)\alpha_y\omega}{U_c}}}{\left(\frac{\alpha_y\omega}{U_c}\right)^2 + \left(\frac{m'_y\pi}{b}\right)^2} \left\{ -\frac{\alpha_y\omega}{U_c} \sin\left[\frac{m'_y\pi(y_{p_1} + b)}{b}\right] - \frac{m'_y\pi}{b} \cos\left[\frac{m'_y\pi(y_{p_1} + b)}{b}\right] \right\} + \frac{e^{\frac{y_{p_1}\alpha_y\omega}{U_c}}}{\left(\frac{\alpha_y\omega}{U_c}\right)^2 + \left(\frac{m'_y\pi}{b}\right)^2} \left[ \frac{\alpha_y\omega}{U_c} \sin\left(\frac{m'_y\pi y_{p_1}}{b}\right) + \frac{m'_y\pi}{b} \cos\left(\frac{m'_y\pi y_{p_1}}{b}\right) \right], \quad (\text{B.16})$$

$$C_{y_8}(\omega, m') = \frac{e^{\frac{(y_{p_1} + b)\alpha_y\omega}{U_c}}}{\left(\frac{\alpha_y\omega}{U_c}\right)^2 + \left(\frac{m'_y\pi}{b}\right)^2} \left\{ \frac{\alpha_y\omega}{U_c} \sin\left[\frac{m'_y\pi(y_{p_1} + b)}{b}\right] - \frac{m'_y\pi}{b} \cos\left[\frac{m'_y\pi(y_{p_1} + b)}{b}\right] \right\} - \frac{e^{\frac{y_{p_1}\alpha_y\omega}{U_c}}}{\left(\frac{\alpha_y\omega}{U_c}\right)^2 + \left(\frac{m'_y\pi}{b}\right)^2} \left[ \frac{\alpha_y\omega}{U_c} \sin\left(\frac{m'_y\pi y_{p_1}}{b}\right) - \frac{m'_y\pi}{b} \cos\left(\frac{m'_y\pi y_{p_1}}{b}\right) \right]. \quad (\text{B.17})$$

For random incident white noise, the external PSD excitation may be defined as

$$S_{\text{ext}} = \frac{4 S_{\text{ref}}}{a b} \left[ \iint_{x_{p_1}}^{x_{p_f}} \sin\left(\frac{m_x\pi x}{a}\right) \sin\left(\frac{m'_x\pi x'}{a}\right) dx dx' \iint_{y_{p_1}}^{y_{p_f}} \sin\left(\frac{m_y\pi y}{b}\right) \sin\left(\frac{m'_y\pi y'}{b}\right) dy dy' \right], \quad (\text{B.18})$$

which analytically developed results in the following expression

$$S_{\text{ext}} = \left[ \frac{4 a b S_{\text{ref}}}{m_x m'_x m_y m'_y \pi^4} \left\{ \cos\left(\frac{m_x\pi(x_{p_1} + a)}{a}\right) - \cos\left(\frac{m_x\pi x_{p_1}}{a}\right) \right\} \left\{ \cos\left(\frac{m'_x\pi(x_{p_1} + a)}{a}\right) - \cos\left(\frac{m'_x\pi x_{p_1}}{a}\right) \right\} \left\{ \cos\left(\frac{m_y\pi(y_{p_1} + b)}{b}\right) - \cos\left(\frac{m_y\pi y_{p_1}}{b}\right) \right\} \left\{ \cos\left(\frac{m'_y\pi(y_{p_1} + b)}{b}\right) - \cos\left(\frac{m'_y\pi y_{p_1}}{b}\right) \right\} \right], \quad (\text{B.19})$$

where  $S_{ref}$  is the constant PSD amplitude of the normally impinging noise on the plate.

### C. Analytical expressions for $S_{ww}(\omega)$ and $S_{pp}(\omega)$ functions

The plate overall displacement PSD function,  $S_{ww}(\omega)$ , was previously defined by Eq. (31). In order to obtain the final analytical expression for this function, one must substitute Eqs. (6) into Eq. (29), and then integrate over the plate area, as shown in Eq. (31). Doing this, the final expression for  $S_{ww}(\omega)$  is

$$S_{ww}(\omega) = \frac{4ab}{\pi^4} \sum_{m_{x1}, m_{x2}=1}^{M_x^2} \sum_{m_{y1}, m_{y2}=1}^{M_y^2} \frac{S_{ww}(\omega)_{m_1, m_2}}{m_{x1} m_{x2} m_{y1} m_{y2}} \cos\left(\frac{m_{x1} \pi x_{p_i}}{a}\right) \cos\left(\frac{m_{x2} \pi x_{p_i}}{a}\right) \cos\left(\frac{m_{y1} \pi y_{p_i}}{b}\right) \cos\left(\frac{m_{y2} \pi y_{p_i}}{b}\right) [\cos(m_{x1} \pi) - 1] [\cos(m_{x2} \pi) - 1] [\cos(m_{y1} \pi) - 1] [\cos(m_{y2} \pi) - 1] \quad (C.1)$$

with each matrix component  $S_{ww}(\omega)_{m_1, m_2}$  corresponding to the respective element of the matrix previously defined in Eq. (24).

Similarly, the analytical expression for the enclosure overall pressure PSD function,  $S_{pp}(\omega)$ , may be obtained by replacing Eqs. (10) into Eq. (30), and then integrating over the enclosure volume, as shown in Eq. (32). It can be shown that the final analytical expression for  $S_{pp}(\omega)$  is

$$S_{pp}(\omega) = \frac{L_x L_y L_z}{8} \sum_{n_{x1}, n_{x2}=1}^{N_x^2} \sum_{n_{y1}, n_{y2}=1}^{N_y^2} \sum_{n_{z1}, n_{z2}=1}^{N_z^2} A_{n_{x1}}^2 A_{n_{y1}}^2 A_{n_{z1}}^2 S_{pp}(\omega)_{n_1, n_2} \quad (C.2)$$

with each matrix component  $S_{pp}(\omega)_{n_1, n_2}$  corresponding to the respective element of the matrix previously defined in Eq. (25).



# Freedom Step

Convert a standard floor to a superior floor with the Freedom Step Acoustical & Impact Isolation Subfloor

**AcustiFloat®**  
Acoustical & Impact Subfloor Systems

WILREP LTD.

Tel. (905) 625-8944 Toll Free 1-888-625-8944

[www.acustifloat.com](http://www.acustifloat.com)

Gym Rooms Playrooms Home Theaters Dance Floors

AcustiFloat is a registered Trademark of WILREP LTD.

# GOAL:

- ✓ REDUCE NOISE
- ✓ REDUCE WEIGHT
- ✓ REDUCE COST
- ✓ INCREASE CUSTOMER PROFITS



# GOAL ACHIEVED.

Blachford specializes in testing, designing and producing quality acoustical materials.

Strategic, fast, flexible and loaded with talent, we bring our customers big-impact solutions. We're a responsive, reliable partner fully committed to continual improvement and well-known for our strengths in technology, innovation and rigorous process.

In the past three years we've saved our customers millions in both costs and in pounds of excess weight. And we've reduced product noise levels an average of 38%. That's something to celebrate.

Featuring state-of-the-art resources and expertise, Blachford is your ideal partner for producing noise control products while improving your bottom line.

**Quality Management System**  
ISO 9001:2000 & ISO/TS 16949

**Environmental Management System**  
Responsible Care (CDN) & ISO 14001 (US)

**Laboratory Management System**  
ISO 17025 for ASTM C423 & SAE J1400

- Engineering
- Designing
- Testing
- Manufacturing

For details call

**630.231.8300**  
or visit us at [blachford.com](http://blachford.com)

**Blachford**